Send Orders for Reprints to reprints@benthamscience.ae

Current Medicinal Chemistry, **2015,** *22,* **1829-1849**

Necrosis Avidity of Organic Compounds: A Natural Phenomenon with Exploitable Theragnostic Potentials

Marlein Miranda Cona, Raymond Oyen and Yicheng Ni*

University Hospitals, K.U. Leuven, Belgium

Yicheng Ni

Abstract: Necrosis is an *in vivo* chaotic event distinguished by uncontrolled disintegration of the cell membrane leading to cytolysis, inflammation and tissue destruction followed by a healing or regenerating process. Targeting necrosis may offer potential diagnostic, therapeutic and/or theragnostic applications in translational medicine. This article reviews the current concept of necrosis including definition, etiology and pathophysiology. The evolution and development of a wide diversity of necrosis targeting agents and their potential applications in preclinical and clinical settings are also elaborated and discussed.

Keywords: Cancer, cardiovascular diseases, diagnosis, necrosis, necrosis avid compounds, treatment.

1. INTRODUCTION

Necrosis has been described as the fortuitous death of cells in a living being having subjected to severe exogenous or endogenous insults [1]. It has been regarded as a passive process of irreversible changes in membrane permeability, organelle breakdown and release of intracellular contents into the extracellular space, which in turn triggers subsequent inflammation and tissue healing [2].

Identifying necrosis by imaging modalities has attracted attention for the management of cardiac pathologies of especially ischemic heart disease. The development of effective agents specific for necrosis and/or ischemia has been a desired goal. In magnetic resonance imaging (MRI), a variety of contrast agents, most of which are based on low molecular weight gadolinium complexes, have been used in clinic [3]. However, inability to distinguish different types of pathologies and a lack of specificity for necrosis has been noted. Categories of porphyrin and non-porphyrin compounds with highly selective, affinity for necrotic tissues have emerged as a potential option for medical applications. These so called necrosis avid contrast agents (NACAs) include paramagnetic metalloporphyrins such as bis-gadolinium-diethylene triamine pentaacetic acid (Gd-DTPA) mesoporphyrin (gadophrin-2) and manganese tetraphenylporphyrin (Mn-TPP) [3-5] as well as nonporphyrin agents such as bis-Gd-DTPA-pamoic acid bis-hydrazide (ECIII-60) and bis-Gd-DTPA-benzylidene-bis-indole (ECIV-7) [3, 4, 6]. In cardiology, the use of these NACAs may provide early localization and depiction of myocardial infarction (MI), patient follow-up, outcome assessment of revascularization therapies [7] and detection of many others cardiac complications and pathologies [8-10]. By using optical imaging, the fluorescent probe hypericin has shown its favorable features for the visualization of MI [11]. In nuclear imaging, diverse "hot spot" imaging tracers with affinity for necrosis have been also tested for MI visualization such as technetium-99m based agents [12, 13], indium-111 labeled antimyosin antibodies [14] and the naphthodianthrone hypericin labeled with iodine-123 [15].

In oncology, a generic and unconventional therapeutic strategy known as OncoCiDia based on necrosis-avidity has recently developed as a complementary approach to improve cancer treatment [16, 17]. Contrary to other targeted cancer therapies directly hitting mutant and resistant tumor cells, OncoCiDia may selectively treat solid cancers by largely eradicating the tumor mass plus radioactively cleansing their microenvironments. It involves two sequential complementary procedures: first a vascular disrupting agent (VDA) [18] is intravenously administered, which is followed by systemic targeted radiotherapy (STR) using a necrosis avid compound (NAC) hypericin labeled with iodine-131 (^{131}I-Hyp). OncoCiDia is meant for managing cancer (Onco) with both tumoricidal (Ci) and diagnostic (Dia) effects. Proof-of-principle studies suggest that this unique approach may provide a simple, practical, reliable and broad-spectrum solution for treating diverse solid cancers [16, 17]. In the meantime, the gamma rays emitted by iodine-131 (^{131}I) allow tumor imaging and therapy follow-up. Thus OncoCiDia constitutes a simultaneous dual targeting theragnostic anticancer modality.

In this review article, the current concept of necrosis and applicability of necrosis as a target for medical diagnostic and therapeutic utilities are discussed (Fig. **1**).

2. BASIC CONCEPTS OF NECROSIS

2.1. Definition and Etiology

Necrosis or type-III cell death is defined as the part of tissue death in a living body. Necrosis has been historically

*Address correspondence to this author at the University Hospitals, K.U. Leuven, Belgium; Tel: 0032-16-330165; Fax: 0032-16-343765;
E-mail: Yicheng.Ni@med.kuleuven.be

0929-8673/15 $58.00+.00

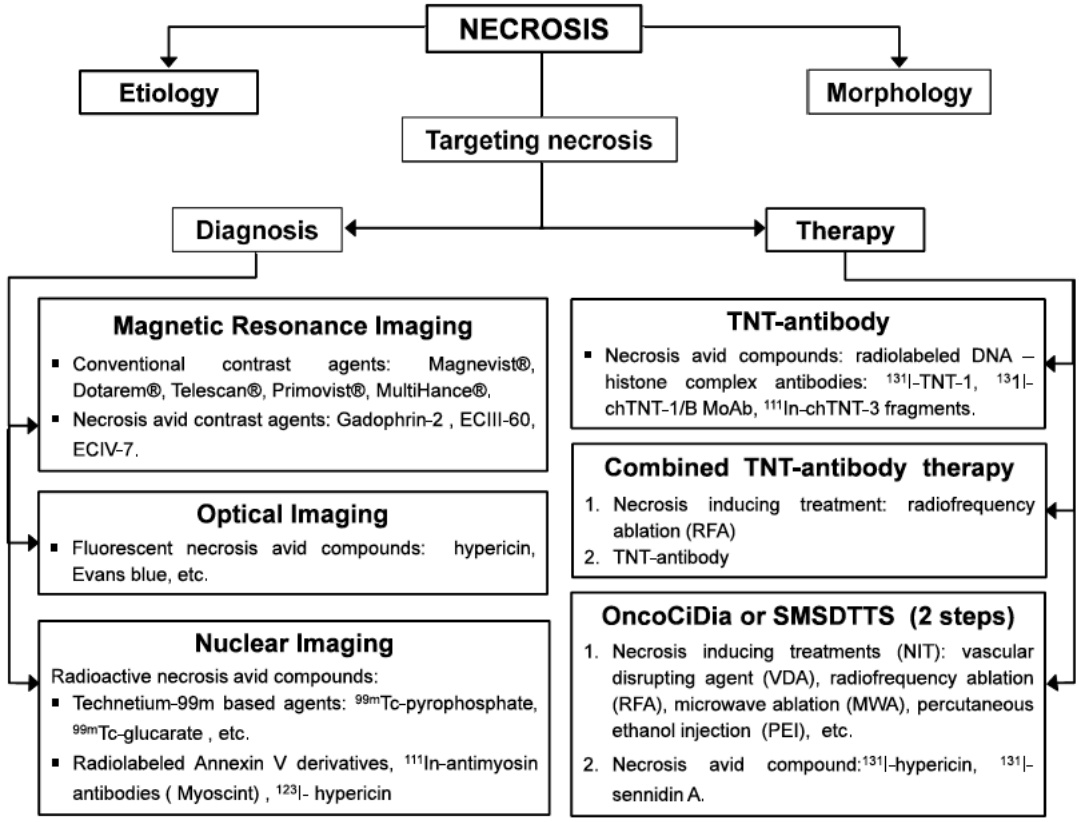

Fig. (1). Flow diagram of the included research topics. DNA: deoxyribonucleic acid, Magnevist®: gadolinium-diethylene triaminepentaacetic acid, Dotarem®: gadolinium-tetraazacyclododecanetetraacetic acid, Gadophrin-2; ECIII-60: bis-Gd- N, N'-bis(diethylenetriaminopentaacetato)-4,4'-methylene-bis (2-hydroxy-3-naphthoic hydrazide); ECIV-7: bis-Gd- N,N'-bis(diethylenetriamine pentaacetic acid)-3,3'-(benzylidene)-bis-(1H-indole-2-carbohydrazide); MultiHance®: gadobenate dimeglumine, Magnevist®: gadopentetate dimeglumine, MoAb: monoclonal antibodies, Primovist®: gadolinium ethoxybenzyl diethylenetriaminepentaacetic acid; Telescan®: manganese - N, N'-dipyridoxylethylenediamine-N, N'-diacetate-5, 5'-bis(phosphate), TNT: tumor necrosis treatment, ^{99m}Tc: technetium, ^{111}In: indium-111, ^{123}I: iodine-123, ^{131}I: iodine-131.

considered as a non-programmed, non-physiological process caused by physicochemical stimuli and/or genetically programmed injuries (Fig. **2**) [2]. Extreme radiation exposure and abnormal temperatures (e.g. < 0°C and > 60°C), high concentrations of chemicals (e.g. toxins, insecticides, and ethanol), oxygen deprivation (e.g. hypoxia and ischemia) and nutritional imbalance can induce necrosis [2]. Genetic reactions and infectious agents (e.g. bacteria, viruses and fungi) have been identified as necrotic pathogens. Neurodegenerative syndromes and pathologies, such as Huntington's disease, Parkinson's disease, and amyotrophic lateral sclerosis [19], may also involve necrosis.

Contrary to apoptosis, which has been identified as an evolutionarily conserved programmed multi-pathway cell-death, necrosis has been stereotyped as an unregulated process [20]. However, recent studies have shown the existence of multiple pathways of a regulated necrotic process, also known as necroptosis. Examples are mitochondrial permeability transition (MPT), poly (adenosine diphosphate-ribose) polymerase 1 (PARP1) hyperactivation, the necrosome, the system cysteine (Cys)-glutamate antiporter, nicotinamide adenine dinucleotide phosphate-oxidase (NADPH) and the inflammasome [21, 22]. Various necroptosis inductors have been also identified including tumor-necrosis factor (TNF), caspase-8 mutations [23], CD95 (Fas/APO-1)-ligand (CD95L), TNF-related weak inducer of apoptosis (TWEAK), TNF-related apoptosis-inducing ligand (TRAIL), genotoxic stresses and certain anticancer drugs. Pathogen-associated molecular patterns (PAMPs), lipopolysaccharide-mediated activation of Toll-like receptor 4 (TLR4), retinoic acid inducible gene I (RIG I)-like receptors (RLRs), and recently, interferons (IFNs) have also shown their necroptosis inducing activities [22]. Regarding the cell death-upstream regulators, unlike apoptosis which is typically mediated by caspase cascade, the necroptotic process does not depend on caspase activity, but on the kinase activity. The involvement of receptor-interacting protein kinase 1 (RIPK1)- and RIPK3-mixed lineage kinase domain-like protein (MLKL) has been identified as the major feature of the necroptotic death pathway [22]. However, recent studies have also revealed emerging regulatory mechanisms such as NETosis, oxytosis, pyronecrosis, ferroptosis and parthanatos that are reported to come about either independently of RIPK1 or RIPK3 or in the presence of RIPK1 or RIPK3 inhibitors (Fig. **2**) [22].

2.2. Pathophysiological Features

Necrosis is morphologically characterized by cytoplasmic granulation, nuclear changes, organelle and/or cellular swelling 'oncosis', plasma membrane rupture and leakage of

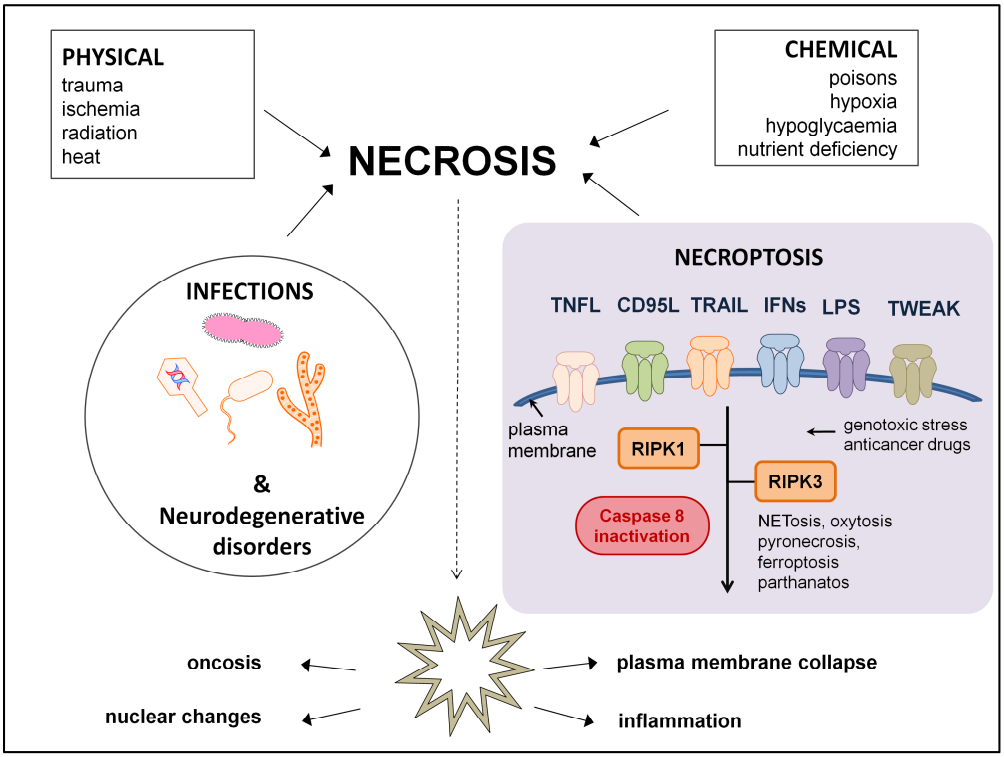

Fig. (2). Simplified scheme of the etiology and morphology of necrosis. Many physicochemical and pathological triggers are involved in the initiation of the necrosis that was initially considered as a uniquely unregulated process. Necroptosis is a form of regulated cell death that can be caused by diverse biochemical stimuli, such as tumor necrosis factor (TNF), CD95L, TNF-related apoptosis-inducing ligand (TRAIL), interferons (IFNs), lipopolysaccharide (LPS) and TNF-related weak inducer of apoptosis (TWEAK), caspase-8 inactivation, genotoxic stress and anticancer drugs. Upon activation, the necroptotic process is driven by receptor-interacting protein kinase 1 and 3 (RIPK1/3). Additional regulator pathways including NETosis, oxytosis, pyronecrosis, ferroptosis and parthanatos have been recently identified. From the morphological point of view, both necrosis and necroptosis share similar features distinguished by oncosis, nuclear changes, plasma membrane collapse and inflammation.

intracellular content (Fig. **2**) [1]. Although necroptotic cell death comes about under regulated conditions, both necroptosis and unregulated necrotic death share similar morphological features distinguished by irreversible changes in the cytoplasm and nucleus of the dead or dying cells [24].

Necrotic cells typically exhibit high levels of eosinophilia due to an increase in the binding of eosin to denatured cytoplasmic proteins and the occurrence of the cytoplasmic RNA-associated basophilia. By electron microscopy, the morphology of dead cells can be clearly distinguished by ruptures in plasma and membranes surrounding the organelles, dilated mitochondrias resembling large amorphous densities, intracytoplasmic myelin figures, unstructured osmiophilic remnants and fluffy material [2]. Eventually, these structures are phagocytosed by other cells or converted into fatty acids whose further calcification contributes to a calcium soap formation [25]. Microscopic observations have shown significant nuclear modifications eventually leading to nuclei dissolution within two days [2]. Dissociation of ribosomes from the endoplasmic reticulum as well as nucleus disintegration with chromatin condensation due to nucleus dissolution (karyolysis), nuclear shrinkage/condensation accompanied with an increase of basophilos (pyknosis) and nucleus rupture (karyorrhexis) occurs [26]. The dead cells eventually fade away because of the combination of enzymatic denaturation and fragmentation process, followed by polymorphonuclear leukocyte phagocytosis of solid particles. Ultimately, the tissue re-grows and the lesion is repaired by regeneration and/or scar formation.

The development of necrotic process requires hours to show detectable alteration at cellular level. Cardiac-specific enzymatic and protein materials from necrotic muscle present in the blood can be detected 2 h after myocardial cell death. In a lethal myocardial infarct where the only pathological indication might be occlusion of a coronary artery, the initial histological evidence of myocardial necrosis is not detectable until 4-12 h later [27].

At early stages of the necrotic process, however, the permeability of plasmalemma allows small charged molecules that normally do not pass through the plasma membrane to enter into the cell [26]. These features permit the use of cell-impermeable dyes for optical imaging of dead or dying cells in tissue cultures. For these purposes, different fluorochrome probes have been used such as propidium iodide (PI), ethidium homodimer-1 (EthD-1), mono- and dimeric cyanine nucleic acids, given their reliability and reproducibility [28-30]. These dyes are basically non-fluorescent in aqueous solution, however show significant enhancement of their fluorescence quantum yield after binding nucleic acids. In addition, double staining with two targeting probes has been applied for discrimination between apoptotic and

necrotic cells in culture tissues [31]. A commercial kit based on fluorescent Annexin V and PI is currently available, in which Annexin V-positive/PI-negative staining is considered as apoptosis and PI-positive staining as necrosis [32]. Dual targeting LIVE/DEAD kits containing PI and membrane-permeant fluorescent probes such as carboxyfluorescein diacetate succinimidyl ester (CFDA-SE), Hoechst-33342, SYBR-14, 4',6-diamidino-2-phenylindole (DAPI) and acridine orange have been also introduced for viability assessment [33, 34], providing a rapid and convenient assay based on fluorescent detection. The simultaneous use of these dyes provides a staining pattern which makes it possible to differentiate normal, apoptotic, and dead cell populations.

Like the necrotizing process itself, the scientific insight into this pathology is still expanding and evolving with new potential medicinal applications constantly explored as detailed in the following sections.

3. NECROSIS TARGETING AS BIOLOGICAL PLATFORM OF DIFFERENT IMAGING TOOLS

Myocardial infarction (MI) is a leading cause of adult mortality and morbidity in developed countries [35]. It usually takes place when the fibrous cap overlying an atherosclerotic plaque in a coronary artery breaks apart. The blood exposed to the atherosclerotic material coagulates forming thrombus or clot, which block the artery and eventually stops the blood flow to a section of the heart muscle [36]. As a result of prolonged myocardial ischemia, irreversible injury and necrosis of myocardial tissues occur.

Necrosis imaging might constitute a valuable approach in the MI management. The development of specific targeting agents with affinity for dead and/or ischemic areas has drawn significant attentions. Such compounds may allow early detection, delineation of the infarcted or ischemic area, patient follow-up over-time and evaluation of the response to revascularization therapies [7]. Other cardiovascular diseases related to cardiac cell death could be detected including diverse cardiomyopathy [8], myocardial inflammation, acute myocarditis [9] and detection of acute or chronic diffuse myocardial damage caused by cardiac transplant rejection [10]

3.1. Magnetic Resonance Imaging (MRI)

3.1.1. Evolution of Contrast Agents (CAs) for Targeting Necrosis

Magnetic Resonance Imaging (MRI) has played an essential role for the localization and assessment of myocardial viability. It is a non-invasive diagnostic technique that offers excellent quality and high-resolution images. However, its relatively low sensitivity in comparison to other techniques (e.g. nuclear imaging) has constrained the introduction of certain agents with magnetic properties for contrast enhancement. Most commonly used contrast agents (CAs) are based on the transition metal ions of paramagnetic properties including gadolinium (Gd^{3+}) and manganese (Mn^{2+}) ions, which own a number of unpaired electron spins in the outer electron shells and a relatively long electron-spin relaxation time. These compounds interact with adjacent water molecules allowing the enhancement of proton relaxation of the hydrogen atoms, and then increasing the contrast among the different structures in the body.

Conventional CAs with "supposed" infarct affinity were introduced in order to generate enhanced images and improve the delineation between normal and diseased myocardium [37]. Low molecular weight gadolinium complexes such as gadolinium-diethylene triamine pentaacetic acid (Gd-DTPA) dimeglumine (Magnevist®, Schering AG, Berlin, Germany) and gadolinium-tetraazacyclododecane tetraacetic acid (Gd-DOTA or Dotarem®, Guerbet, France) are the most commonly used [38]. However, uncertainties were noted due to insufficient discrimination between different cardiac diseases, e.g. reversibly versus irreversibly damaged myocardium, acute versus chronic myocardial infarction (MI), and ischemic versus inflammatory lesions [39]. Non-selective enhancement of necrotic tissues, wash-in and washout kinetic patterns and main elimination route through the kidneys were observed [3]. As a consequence, nephrogenic fibrosing dermopathy due to the prolonged tissue retention of the bio-incompatible metal gadolinium was clinically confronted in patients with prior renal dysfunction when some of such agents are used [40]. Phosphonate-modified Gd-DTPA complexes were an interesting alternative characterized by long-term images with high contrast enhancement in diffuse and occlusive MI pathologies. They interact with calcium-rich tissues causing "in situ" formation and precipitation of the insoluble calcium phosphate within the injured cardiomyocytes. Nevertheless, overestimation of non-viable lesion size due to lack of specificity between ischemic and necrotic areas or unwanted effects like calcium-homeostasis disorder and consequently impaired ventricular contractility remain concerns for clinical use [41].

A second generation of CAs was developed and nowadays are commercially available including manganese - N, N'-dipyridoxylethylenediamine-N, N'-diacetate-5, 5'-bis(phosphate), (Mn-DPDP or Teslascan®; GE Healthcare, Milwaukee, WI, USA) [42] gadolinium ethoxybenzyl diethylenetriaminepentaacetic acid (Gd-EOB-DTPA or Primovist®; Bayer Schering Pharma AG, Berlin, Germany) [43] and gadobenate dimeglumine (Gd-BOPTA or MultiHance®; Bracco Imaging SpA, Milan, Italy) [44], but they are mainly intended for liver imaging due to their major hepatobiliary metabolic pathways.

3.1.2. Necrosis Avid Contrast Agents (NACAs): Structural Diversity Versus Common Targetability

Necrosis avid contrast agents (NACAs) originally represented a novel group of porphyrin compounds identified by Ni *et al.* [3, 45]. They were conceived as MRI necrosis-targeting agents to identify acute MI, assess tissue viability, and evaluate therapeutic outcomes after interventional treatments. Additional functions like hepatobiliary, adrenal and splenic contrast enhancement, first-pass perfusion, blood pool contrast effect, and renal functional imaging were also demonstrated with NACAs [4, 6].

3.1.2.1. Porphyrin-Based NACAs

Porphyrins are a group of organic compounds found in plants and animals as key functional life molecules such as hemoglobin, hematoporphyrin, membrane-bound hemopro-

teins, chlorophylls and cobalamin (vitamin B-12) (Fig. **3**). Structurally, they are based on an aromatic heterocyclic macrocycle containing four pyrrole moieties coupled by methine bridges (=CH-) with a central binding site for metal coordination (Fig. **3**). The extensive conjugation across alternating multiple and single bonds amongst adjacent parallel aligned p-orbitals of the atoms produce electron delocalization conferring an intense chromaticity, being called "porphyrin", greek term derived from purple. Paramagnetic metalloporphyrins are synthesized by means of the coordination with transition metal ions such as Gd^{+3} and Mn^{+2}.

After multi-institutional reproducibility studies, the Gd-chelated porphyrin gadophrin-2 (mesoporphyrin-IX-13,17-bis(2-oxo-4,7,10,10-tetra(carboxylatomethyl)-1,4,7,10-tetraazadecyl) diamide, digadolinium complex, disodium salt) was accepted as a necrosis targeting MRI contrast agent due to its high necrosis-avidity and specific uptake in myocardial infarction [4, 6]. Chemical modifications of gadophrin-2 structure by hosting a copper ion into the core of the cyclic tetrapyrrole ring lead to gadophrin-3 with superior structural stability and safety [46]. However, their commercial introduction was abandoned by the pharmaceutical companies due to their presumed clinical intolerance and unwanted effects related to the chemical nature and phototoxicity [3].

3.1.2.2. Non Porphyrin-Based NACAs

The correlation between the cyclic tetrapyrrole structure of porphyrins and targetability was investigated. Four out of nine metalloporphyrins lacked of necrosis avidity, suggesting the tetrapyrrole ring is unlikely a structural prerequisite for the specific targetability [3, 4]. Mono, bis-, and tri-pyrrole derivatives as well as open chain tetrapyrroles were evaluated, showing no convincing necrosis-specificity [3]. These findings opened the possibilities to generate non-porphyrin based NACAs with lighter color and without unwanted side-effects associated with porphyrin-based compounds. Indeed, two potential NACAs, the light yellowish bis-Gd- N, N'-bis(diethylenetriaminopentaacetato)-4,4'-methylene-bis (2-hydroxy-3-naphthoic hydrazide) (bis-Gd-DTPA pamoate or ECIII-60) and the colorless bis-Gd- N,N'-bis(diethylenetriamine pentaacetic acid)-3,3'-(benzylidene)-bis-(1H-indole-2-carbohydrazide) (bis-Gd-DTPA benzylidene-bis-indole or ECIV-7) were synthesized [4, 6] having extraordinary necrosis avidity and excellent properties for medical purposes (Fig. **4**). The former is derived from pamoic acid, which is a common matrix for pharmaceutical preparations [47]. The latter is an indole derivative that partially simulates catabolic metabolites of organisms [48]. Unfortunately, after completing the last reserved batch in our recent preclinical oncological study [49], non-porphyrin NACAs for MRI became momentarily unavailable because of human

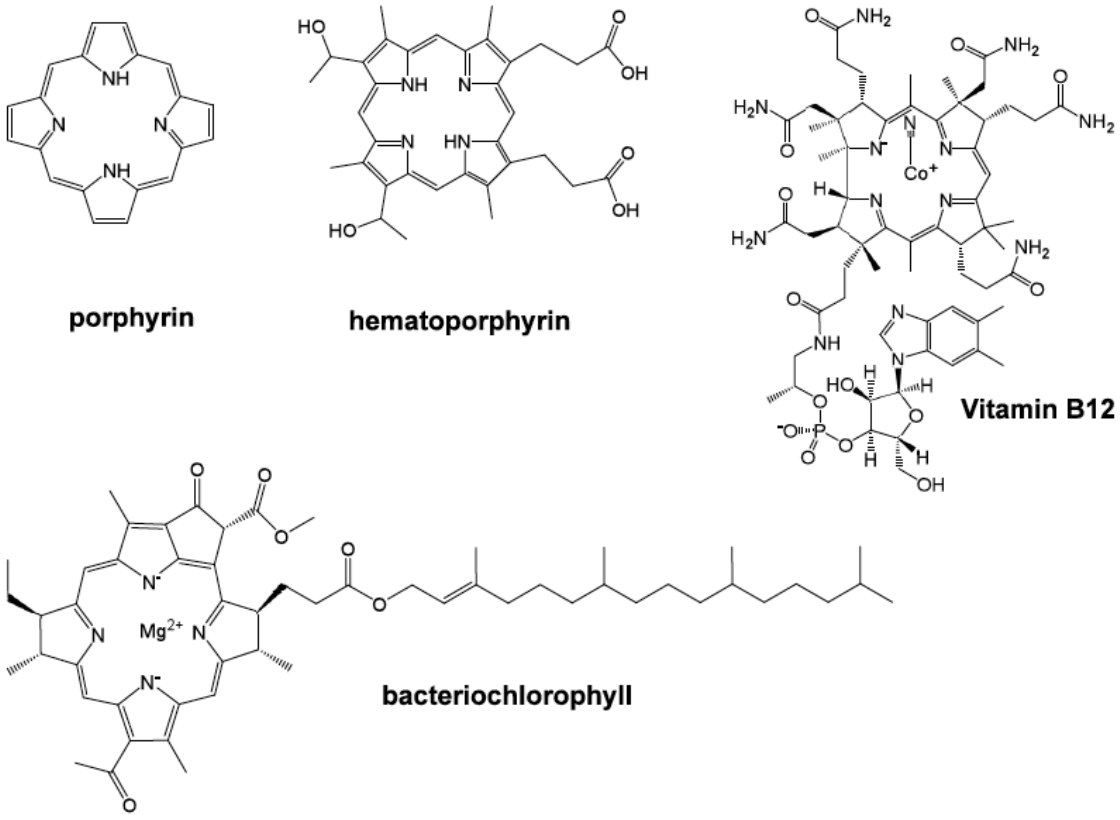

Fig. (3). Schematic representation of the typical chemical structure of porphyrin consisting of aromatic heterocyclic compound with four pyrrole moieties coupled by methine bridges and a central site for metal coordination. Pophyrin compounds enclose functional life molecules such as 7,12-bis(1-hydroxyethyl)-3,8,13,17-tetramethyl-21H,23H-porphine-2,18-dipropanoic acid (hematoporphyrin), α-(5,6-dimethylbenzimidazolyl) cobamidcyanide (vitamin B12) and magnesium,[3,7,11,15-tetramethyl-2-hexadecenyl-9-acetyl-14-ethyl-13,14-dihydro;-21-(methoxycarbonyl)-4,8,13,18-tetramethyl-20-oxo-3-phorbinepropanoato(2-)-n23 (bacteriochlorophyll).

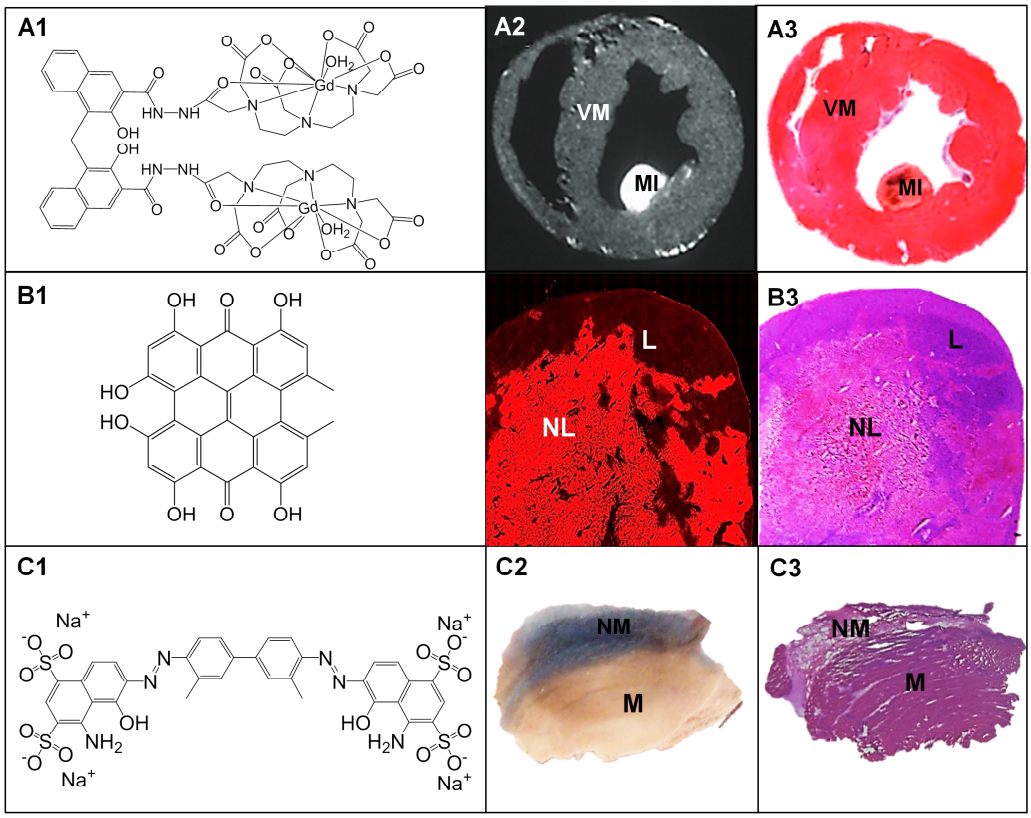

Fig. (4). Schematic representation of necrosis avid compounds and their selective affinities for necrotic tissues. **A1-A3**: *Ex vivo* analysis of bis-gadolinium-diethylene triaminepentaacetic acid-pamoic acid bis-hydrazide (ECIII-60) (**A1**) in a dog with a small acute myocardium infarction involving only posterior papillary muscle. The NAC ECIII-60 caused a precise, strong and persistent contrast enhancement on T1-MRI even 24h after intravenous injection (**A2**) at a 1.5-T magnet, as proven by TTC histochemical staining (**A3**). **B1-B3**: Post-mortem analysis of necrotic and viable hepatic tissues from rats with reperfused partial liver infarction (RPLI) having received the napthrodianthone hypericin (**B1**). Macroscopic images of 50-µm-thick sections (**B2**) and histology co-localization (**B3**) showed the selective affinity of the highly fluorescent hypericin for necrotic liver contrary to the low fluorescence found in viable liver. **C1-C3:** Post-mortem study of necrotic and viable tissues from rats with ethanol-induced muscle necrosis pre-injected with Evans blue dye (**C1**). The necrotic muscle retained Evans blue as blue hyper intense areas, with normal muscle without staining (**C2**), as was confirmed by histology (**C3**). MI: myocardium infarction, VM: viable myocardium, NM: necrotic muscle, M: muscle, NL: necrotic liver, L: liver.

reasons beyond the authors' control [49]. Recent efforts seem promising to recover them (data to be published).

In addition to the abovementioned porphyrin and nonporphyrin NACAs, there seems to be a wide diversity in structures and molecular sizes of synthetic or natural compounds, which share common necrosis avidity [3] and have been eventually so-called as necrosis avid compounds (NACs). From small molecules like organic dyes or monosaccharide derivatives (MW~500 g/mol) (Table **1**) to large-size monoclonal antibodies fragments (MW~50 000 g/mol) or protein based compounds (Table **2**), all they might bind to components present in the necrotic debris, such as phospholipids and protein residues in dead cells (Fig. **5**). This wide diversity of compounds with apparently different mechanism of necrosis targetability has opened up new opportunities beyond traditional target-specific agents for diagnosis and/or therapy in cardiology and oncology fields (Table **3**).

3.2. Optical Imaging

Optical imaging (OI) utilizes fluorescent probes and luminescent labels and has been exploited for identifying necrotic tissues. The 1,3,4,6,8,13-hexahydroxy-10,11-dimethylphenanthro [1,10,9,8-opqra]perylene-7,14-dione (hypericin) is a fluorescent, red-colored anthraquinone-derivative (naphthodianthrone) that can be isolated from the perennial herb Hypericum perforatum L (St. John's Wort) (Fig. **4**) [50] or chemically synthesized. Over decades, it has attracted medical interests due to its broad spectrum of biological and pharmacological properties such as antimicrobial, antiviral, antidepressant, antitumor and anti-inflammatory activities [51]. Recently, it has been found with a selective and outstanding affinity for necrotic cell debris (Fig. **4**) [3, 15]. Although the mechanism underlying its necrosis avidity is still unknown, several potential binding pathways have been proposed including low-density lipoproteins (LDL), albumins and cell membrane lipids such as cholesterol, PE and PS [52]. Upon excitation with specific wavelength of light by lasers such as 488 nm (Argon) and 543 nm (Helium-Neon) or by light xenon arc lamp at 380-450 nm or 375-400 nm [53], hypericin shows very strong fluorescent properties in the orange-red region (600–650 nm). By exploiting this feature, it has been recently tested as a viability marker in a rat model of MI for its potential to determine myocardial viability [11].

Table 1. Examples of small molecule necrosis avid compounds, their molecular weights and chemical structures.

Small Molecule-NACs	MW (g/mol)	Chemical Structure
mesoporphyrin-IX-13,17-bis(2-oxo-4,7,10,10-tetra (carboxylatomethyl)-1,4,7,10-tetraazadecyl) diamide, digadolinium complex, disodium salt (Gadophrin-2)	1759.38	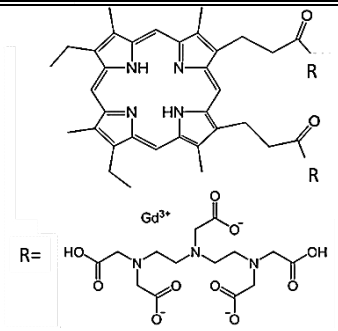
1,3,4,6,8,13-hexahydroxy-10,11-dimethylphenanthro[1,10,9,8-opqra]perylene-7,14-dione (Hypericin)	504.4	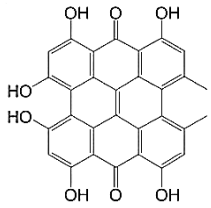
tetrasodium (6E,6'E)-6,6-[(3,3'-dimethylbiphenyl-4,4'-diyl)di(1E)hydrazin-2-yl-1-ylidene]bis(4-amino-5-oxo-5,6-dihydronaphthalene-1,3-disulfonate) (Evans blue)	960.82	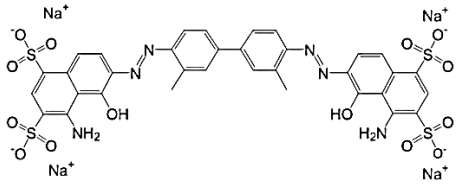
^{99m} technetium- 99m-glucarate	530.15	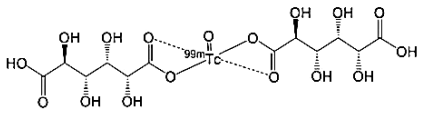
Duramycin from Streptoverticillium cinnamoneus	2013.28	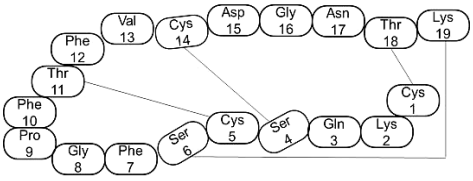
4-[(3-carboxy-2-hydroxynaphthalen-1-yl)methyl]-3-hydroxynaphthalene-2-carboxylic (pamoic acid)	388.87	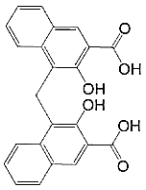
3,3′-(benzylidene)-bis-(1H-indole-2-carbohydrazide) (bis-indole)	438.0	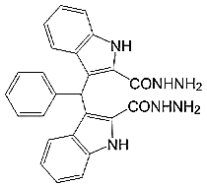

MW: molecular weight, NACs: necrosis avid compounds, Ala: alanine, Asn: asparagine, Asp: aspartic acid, Cys: cysteine, Gly: glycine, Gln: glutamine, Lys: lysine, Phe: phenylalanine, Pro: proline, Ser: serine, Thr: threonine, Val: valine.

Table 2. Examples of protein structure based necrosis avid compounds, their molecular weights and schematic representation of their chemical structures.

Protein Structure Based- NACs	MW (g/mol)	Chemical Structure
Imciromab pentetate Fab	~50 000	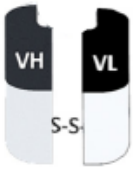
Annexin V	36 000	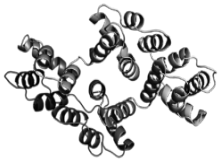
C2A domain of synaptotagmin I	12 000	

Fab: fragment, antigen-binding region of a monoclonal antibody, VH: variable heavy chain, VL: variable light chain, S-S: disulfide bridge, MW: molecular weight, NAC: necrosis avid compound.

The tetrasodium (6E,6'E)-6,6-[(3,3'-dimethylbiphenyl-4,4'-diyl)di(1E)hydrazin-2-yl-1-ylidene]bis(4-amino-5-oxo-5,6-dihydronaphthalene-1,3-disulfonate) (Evans Blue) is a blue dye that is produced by reacting 4-(4-Amino-3-methylphenyl)-2-methylaniline (o-tolidine) with 1-amino-8-naphthol-2,4-disulfonic acid (Chicago acid) [54]. Over the years, it has been used for intravital staining of plasma leakage owing to its high affinity to plasma proteins at a molar ratio of 10:1 [55]. However, more recently, its affinity for cell death has been experimentally evidenced, making it a good optical imaging tracer for severe tissues damage (Fig. **4**). Necrotic lesions in skeletal myofibres have been properly identified with Evans Blue in a treadmill-exercised mdx mouse model of human Duchenne muscular dystrophy by three-dimensional optical coherence tomography (3D-OCT) [56]. In more recent studies on biodistribution and tumoricidal effects of the necrosis avid radioiodinated Hyp in nude mice bearing radiation-induced fibrosarcoma (RIF-1) tumors, rats of reperfused liver infarction (RLI) and rats with hepatic rhabdomyosarcoma (R1), systemic injections of Evans Blue have been administered to assist in distinguishing necrotic areas over viable tissues [57, 58]. A similar approach was used in a study on identification of critical components of myocardial infarction (MI) including area at risk, MI-core and salvageable zone in rabbits by cardiac MRI [59].

3.3. Nuclear Imaging

Nuclear scintigraphy presents the most sensitive diagnostic imaging techniques. It uses radiolabelled tracers or compounds recognizing specific structures, receptors or antigens to scrutinize the molecular process under *in vivo* conditions in a noninvasive manner. A wide diversity of "hot spot" NACs have been exploited for the visualization of myocardial infarction (MI) by nuclear imaging techniques such as positron emission tomography (PET) and single-photon emission computed tomography (SPECT).

3.3.1. Necrosis Avid Tracers

3.3.1.1. Small Molecule - NACs

The first agent used, technetium-99m (^{99m}Tc)-pyrophosphate, concentrated in necrotic myocardium by targeting the calcium phosphate present in the mitochondria of infarcted or harshly damaged myocardium [13]. Nevertheless, its poor specificity for distinguishing ischemic and

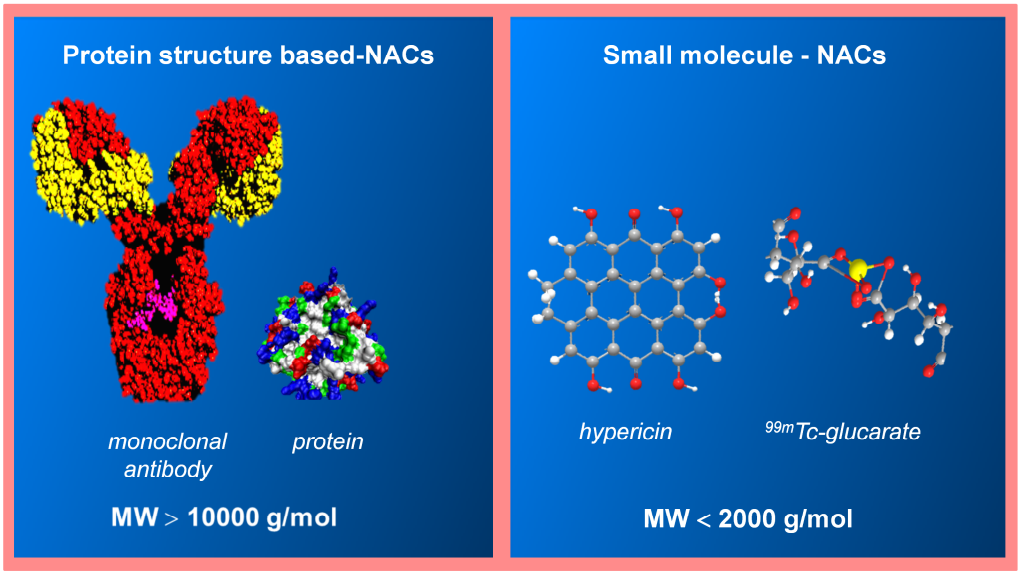

Fig. (5). Three-dimensional representation of examples of necrosis avid contrast agents such as a monoclonal antibody, a protein domain, the naphtodianthrone hypericin and the ^{99m}Tc-labeled glucarate, showing their wide diversity in structure and molecular size.

Table 3. Examples of necrosis avid compounds, their proposed interaction mechanism and potential clinic applications.

Necrosis Avid Compounds (NACs)	Proposed Mechanism	Applications and Potentialities
Small molecule - NACs		
Gd-chelated porphyrin gadophrin-2	plasma albumin	MI detection with MRI
Hypericin	low-density lipoproteins, albumin, cholesterol, PE and PS	MI detection or therapeutic evaluation after interventional therapies with SPECT using ^{123}I-hypericin. Treatment of solid tumors using ^{131}I-hypericin
Sennidin A	cell debris	Therapeutic evaluation after interventional therapies using ^{123}I- Sennidin A
Evans blue	albumin	Optical imaging of dead tissues in pre-clinical studies like identification of area at risk in MI, MI-core and salvageable zone
^{99m}Tc-glucarate	protein histones in denatured nuclei	MI detection with MRI
Duramycin (DUR)	PE	MI detection with SPECT using ^{99m}Tc-HYNIC-DUR
Pamoic acid (PA)	exposed intracellular protein in damaged cell membrane	MI detection with SPECT, PET and MRI using radiolabeled and Gd (III)-DOTA/DTPA-PA derivatives
bis-indole (BI)	intracellular debris after cell damage	MI detection with SPECT, PET and MRI using radiolabeled and Gd (III)-DOTA/DTPA- BI derivatives
Protein structure based-NACs		
Imciromab pentetate Fab	cardiac myosin of damaged cells	MI detection with SPECT with ^{111}In and ^{99m}Tc-labelled imciromab pentetate
Annexin V	PS	MI detection with SPECT and PET using radiolabeled annexin V derivatives
C2A domain of synaptotagmin I (C2A)	PS	MI detection with SPECT with ^{99m}Tc-labelled C2A

DOTA: 1,4,7,10-tetraazacyclododecane-1,4,7,10-tetraacetic acid, DTPA: diethylene triamine pentaacetic acid, Gd: gadolinium, HYNIC: hydrazinonicotinamide, ^{111}In-indium-111, MI: myocardial infarction, MRI: magnetic resonance imaging, PE: phosphatidylethanolamine, PS: phosphatidylserine, PET: Positron emission tomography, SPECT: Single-photon emission computed tomography, ^{99m}Tc-Technetium-99m

necrotic tissues [60] might cause overestimation of the infarct size [61]. Also, its low *in vivo* stability led to the release and circulation of free pertechnetate and eventually reduced diagnostic accuracy and low target-to-background ratio on scintigraphic images [15].

Glucaric acid or glucarate is a 6-carbon dicarboxylic acid obtained from the oxidation of glucose with nitric acid. The formed complex between glucarate and ^{99m}Tc (Fig. **5**) has been tested as a necrosis-seeking agent owing to its preferential accumulation into basic protein histones within denatured nuclei and subcellular organelles in the dead cardiomyocytes [13]. It shows fast blood clearance, low toxicity and low antigenicity, making it an attractive diagnostic agent for irreversible injury in myocardium. However, ^{99m}Tc-glucarate only accumulates at early stages of tissue damages because of the prompt histone degradation [15].

Duramycin is a tetracyclic 19–amino acid peptide produced by Streptoverticillium cinnamoneus [62]. DUR has a 3-dimensional lipophilic binding site through which it binds the phosphoaminolipid phosphatidylethanolamine (PE) [62] with exclusive specificity and high affinity at a molar ratio of 1:1 [63]. PE represents around 20% of all phospholipids in mammalian cell membranes and, like phosphatidylserine (PS), is merely located at the cytosolic side of the cell membrane [64]. In necrosis, PE becomes accessible to the extracellular surface due to loss of plasma membrane integrity that makes it as a potential molecular target for cell death imaging. In a former study, promising results were obtained by using ^{99m}Tc-HYNIC DUR derivative as PE-specific agent using an *in vivo* rat model of myocardial ischemia and reperfusion [65]. In a recent report, a 1,4,7,10-tetraazacyclododecane-1,4,7,10-tetraacetic acid (DOTA) DUR conjugate was synthetized, characterized and labeled with ^{68}Ga to develop a cell death biomarker for the highly sensitive technique of positron emission tomography (PET) imaging. The radiolabelled peptide was assessed by liposome- and cell-based assays and in tumor-bearing mice undergoing anti-cancer therapy. Overall, promising results were obtained for the assessment of therapeutic efficacy in rodents, suggesting its potential applicability as preclinical candidate for cell death imaging [66].

The potential usefulness of radioiodinated hypericin (mono-[^{123}I] iodohypericin), a radioactive derivative of the potent necrosis avid hypericin has also proved its potential for the detection and quantification of acute myocardial infarction (MI) in infarcted rabbits by using single-photon emission computed tomography (SPECT) imaging (Fig. **6**) [15, 67], in addition to its oncological applications as de-

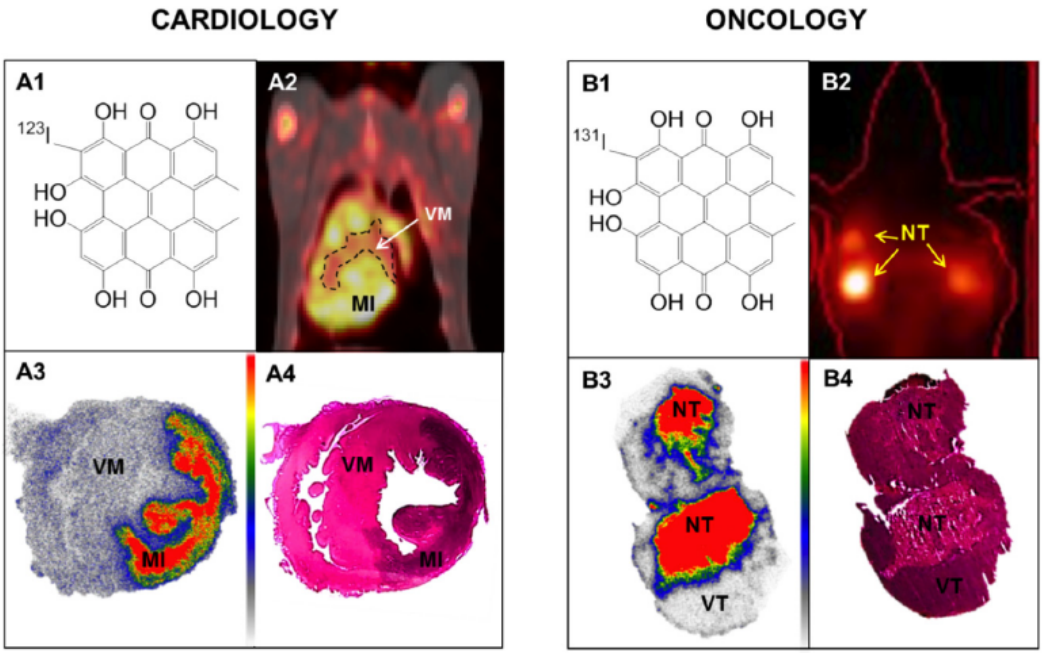

Fig. (6). Potential Theragnostic applications by targeting necrosis for cardiology and oncology. **A1-A4:** Coronal single-photon emission computed tomography-computed tomography (SPECT/CT) images of a rabbit with a massive acute MI having received mono-[^{123}I]iodohypericin (**A1**). The image shows high radioactivity uptake in the MI along with radioactivity in the blood pool including the left ventricular cavity and large blood vessels. Lower uptake in normal myocardium was observed (dashed line delineated dark area & white arrow) (**A2**). A typical autoradiogram of 50-µm-thick sections on short axis cardiac sections corroborates the preferential tracer accumulation in dead areas than in normal myocardium (**A3**)*. Histology analysis confirms the location of the viable myocardium and the infarcted areas distinguished by scattered haemorrhage (**A4**). **B1-B4:** SPECT, autoradiography and histology of multifocal radiation-induced fibrosarcoma-1 (RIF-1) from severe combined immunodeficiency (SCID) mice previously injected with CA4P to induce tumor necrosis followed 24h later with mono-[^{131}I]iodohypericin. Twelve days after radioactivity administration, a high radioactivity accumulation was seen mostly inside the tumor necrosis (yellow arrows). Autoradiograpic (**B3**)* and histologic (**B4**) analysis of the tumor after one month of radioactivity injection perfectly match with the hotspots on tumors (**B2**). *Red colour indicates areas with the highest radioactivity accumulation while white represent the lowest values. MI: myocardium infarction, VM: viable myocardium, NT: necrotic tumour, VT: viable tumour.

scribed in the next section. In an effort to further enhance the biodistribution and clearance properties of the very lipophilic radioiodinated hypericin, other derivatives were also developed by slightly modification of its chemical structure including mono-[^{123}I] iodoprotohypericin [68] and mono-[^{123}I]iodohypericin monocarboxylic acid [69] (Fig. **7**). Although these radioiodinated compounds show their suitability for the detection of necrotic regions, the radionuclide technetium (^{99m}Tc) was also considered for hypericin because of its better availability and lower cost than those of ^{123}I [70]. By linking hypericin with the bifunctional chelating agent, mercaptoacetyldiglycyl-1,5-diaminopentylene, a new tracer agent was obtained and then conjugated to the radiometal ^{99m}Tc (Fig. **7**). However, unlike the radioiodinated hypericin derivatives, it did not exhibit selective necrosis avidity for necrotic regions within subcutaneous RIF-1 tumors from C3H mice. It seems the conjugation of hypericin with a ^{99m}Tc-chelate, resulting in changes in molecular size, electric charge and lipophilic properties, might considerably affect the targetability of this tracer agent. Indeed, in a different study, ^{64}Copper (^{64}Cu)-labeled bis-DOTA conjugated hypericin (^{64}Cu-bis-DOTA hypericin) was synthesized (Fig. **7**) and used to assess the response of xenograft human BT474 breast carcinoma cell tumors in nude mice after being treated with photothermal ablation (PTA) therapy in presence of copper sulfide nanoparticles (CuS NPs). A reduced affinity of ^{64}Cu-bis-DOTA hypericin for necrosis in comparison with the radiodinated Hyp was also observed [71].

Similar to hypericin, the abovementioned optical imaging tracer EB was previously labeled with ^{99m}Tc to be tested as a lymphoscintigraphic agent *in vivo* [72]. Although this application is not related with necrosis detection, future studies with ^{99m}Tc-labeled Evans Blue in animal models of necrosis need to be done that might offer an alternative radioactive agent for imaging necrosis.

3.3.1.2. Protein Structure Based-NACs

Imciromab pentetate (monoclonal antimyosin antibody Fab; ~50 000 g/mol) is a mouse monoclonal antibody antigen binding fragment (Fab) derivative that specifically localizes in the intracellular human heavy chain of the exposed cardiac myosin of severely damaged cells [13]. After Food and Drug Administration (FDA) approval, anti-myosin Fab conjugated to diethylene triamine pentaacetic acid (DTPA) radiolabeled with Indium-111 (^{111}In) under the name Myoscint was used in clinic as an imaging agent for the detection of heart tissue death following MI [73]. Similarly, the monoclonal antimyosin antibody linked to ^{99m}Tc was also tested in patients suffering MI. Safety profile and high sensitivity in imaging detection of both Q-wave and non-Q-wave

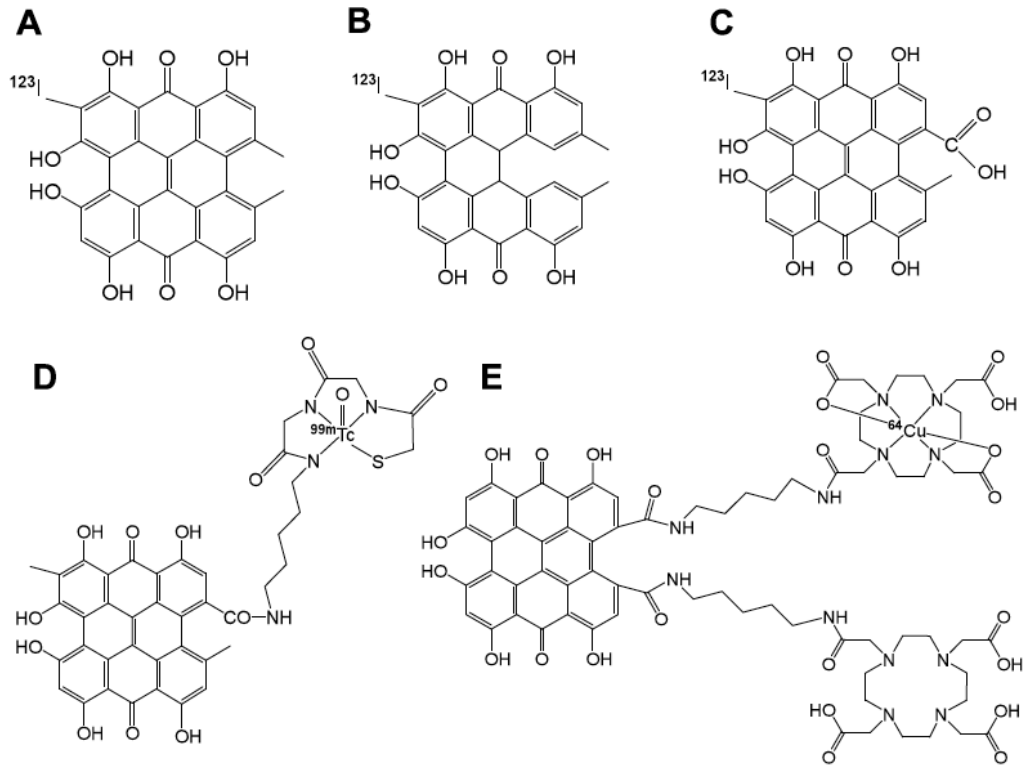

Fig. (7). Chemical structures of the necrosis avid agent 1,3,4,6,8,13-hexahydroxy-2-[^{123}I]iodo-10,11-dimethylphenanthro[1,10,9,8-opqra]perylene-7,14-dione (mono-[^{123}I]iodohypericin) **(A)** and its derivatives including 1,3,4,6,8,15-hexahydroxy-2-[^{123}I]iodo-10,13-dimethyldibenzo[a,o]perylene-7,16-dione (mono-[^{123}I]iodoprotohypericin) **(B)**, 1,6,8,10,11,13-hexahydroxy-2-[^{123}I]iodo-4-methyl-7,14-dioxo-7,14-dihydrophenanthro[1,10,9,8-opqra]perylene-3-carboxylic acid (mono-[^{123}I]iodohypericin monocarboxylic acid) **(C)**, technetium-99m- mercaptoacetyldiglycyl-1,5-diaminopentylene-1,3,4,6,8,13-hexahydroxy-10,11-dimethylphenanthro[1,10,9,8-opqra]perylene-7,14-dione carboxamide ([^{99m}Tc]-hypericin) **(D)**, copper-64-bis-1,4,7,10-tetraazacyclododecane-N,N',N,N'-tetraacetic acid-1,3,4,6,8,13-hexahydroxy-10,11-dimethylphenanthro[1,10,9,8-opqra]perylene-7,14-dione ([^{64}Cu]-bis-DOTA-hypericin) **(E)**.

MI even at the early stage were observed [74]. However, the commercial production of monoclonal antimyosin antibody Fab has been discontinued owing to the reduced number of FDA-approved indications, constrained only to the detection of ischemic heart disease [15].

Annexin V is a member of the annexin family of calcium-dependent phospholipid binding proteins and was firstly isolated from human placenta. Phosphatidylserine (PS) is a negatively charged aminophospholipid typically found at the plasma membrane inner leaflet but it becomes exposed to the outer surface on apoptotic and necrotic cells. Since annexin V specifically binds externalized PS with a high affinity (Kd = 7.0 nM) [75], annexin-based radiotracers can be used for detection of apoptosis and necrosis. A wide variety of annexin V derivatives labeled with different radionuclides such as ^{99m}Tc, ^{111}In, iodine-124 (^{124}I), carbon-11 (^{11}C), gallium-68 (^{68}Ga) and fluorine-18 (^{18}F) have been developed and pre-clinically evaluated using *in vitro* platforms and/or different animal models [75]. In clinical research, however, ^{99m}Tc-6-hydrazinopyridine-3-carboxylic acid (HYNIC)-annexin V derivatives are the only used so far, mainly in patients with ischemia-associated diseases/ conditions and chemotherapy/radiation therapy-induced cell death in certain types of cancers [76].

C2A domain of synaptotagmin I (C2A) is a protein mainly located within the synaptic vesicle membranes that bind to negatively charged phospholipids, including PS, in a Ca^{2+} ion -dependent manner. In previously reported studies, the C2A was fused to glutathione S-transferase and radiolabelled with ^{99m}Tc leading to ^{99m}Tc-C2A-GST for imaging of cell death in rat and pig models of acute MI [77] or in a mouse model of non-small-cell lung carcinoma (NSCLC) after paclitaxel chemotherapy [78]. Increased ^{99m}Tc-C2A-GST uptake was seen either in the myocardial infarcts or in treatment-induced cell death within NSCLC tumors. Similar results were obtained with a fluorine-18 labeled derivative of C2A-GST in a rabbit model of lung cancer after paclitaxel chemotherapy [79].

3.3.1.3. Radioactive NACs Based on MRI-NACAs Results

Based on the previous promising results obtained with both bis-Gd-DTPA-pamoic acid bis-hydrazide (ECIII-60) and bis-Gd-DTPA- benzylidene-bis-indole (ECIV-7) for MRI, a number of radiolabelled derivatives of these compounds were developed.

Two ^{99m}Tc-tricarbonyl complexes of pamoic acid derivatives were synthesized and evaluated in animal models of necrosis (Fig. **8**). The lipophilic ^{99m}Tc-tricarbonyl-[N-(5-aminopentyl)pyridin-2-yl-methylamino]methylacetato-4,4'-methylene-2-hydroxy-3-napthalene carboxamide-(2'-hydroxy-3'-naphthoic acid methyl ester) showed no affinity for necrotic tissues and hepatobiliary pathway as main elimination route. In contrast, the more polar ^{99m}Tc-tricarbonyl

complexes of N, N'-bis(diethylenetriaminopentaacetato)-4,4'-methylene bis(2-hydroxy-3-naphthoic hydrazide) (^{99m}Tc(CO)$_3$-bis-DTPA-pamoate) exhibited affinity and specificity for necrotic areas being eliminated via both the kidneys and the liver. In a further study, a ^{68}Ga labeled bis-DTPA-pamoate derivative was developed for *in vivo* detection of dead areas (Fig. **8**). The presence of acyclic DTPA allowed the conjugation of the compound with the generator produced positron emitter ^{68}Ga to be used as an imaging agent in the highly sensitive PET. However, a limited *in vivo* stability was observed, most likely because DTPA is not an appropriate chelator for ^{68}Ga, leading to a distorted organ distribution and high blood pool activity [80]. In a later study, pamoic acid bis-hydrazide was conjugated to the macrocyclic ligand DOTA to improve the stability and biodistribution with the previous reported bis-DTPA derivate. After labeling with ^{68}Ga, the resulting derivative ^{68}Ga-bis-DOTA-pamoate (Fig. **8**) revealed high *in vivo* stability, selective accumulation in necrotic tissue and a more favorable biodistribution [81].

With benzylidene-bis-indole, a ^{99m}Tc-tricarbonyl complex of bis-DTPA derivative was also synthesised (Fig. **9**) and studied on animal models of necrosis. Results indicated that it could selectively concentrate in dead regions. In a more recent study, a ^{68}Ga labeled bis-DOTA derivative of benzylidene-bis-indole was developed (Fig. **9**) and evaluated in a mouse model of Fas-mediated hepatic apoptosis in correlation with histochemical stainings. The tracer proved to be stable *in vivo* and selective avidity for necrotic cell death [82].

The uptake mechanisms underlying these radiolabelled compounds in necrotic tissue still remain unknown. A possible hypothesis suggests that these tracers interact with an intracellular protein that is denatured and exposed after the loss of the plasma membrane integrity throughout the cell death process [81, 82].

4. TARGETING NECROSIS FOR THERAGNOSTIC APPLICATIONS IN ONCOLOGY

4.1. Cancer Therapies Based on Necrosis

Cancer is one of the most common global life threats and includes a complex group of over 200 malignant diseases that can be caused by both genetic and environmental risk factors. Over the last decades, an escalated increase in prevalence and incidence of cancer has been noticed worldwide.

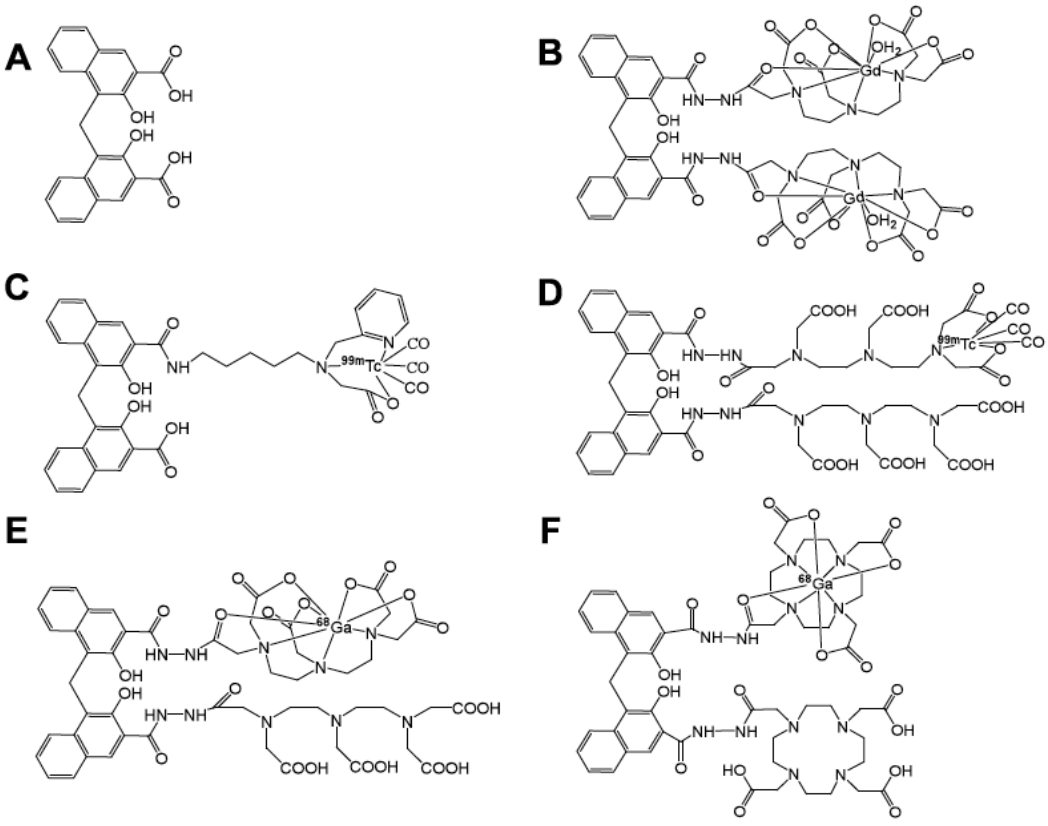

Fig. (8). Schematic representation of the chemical structures of 4-[(3-carboxy-2-hydroxynaphthalen-1-yl)methyl]-3-hydroxynaphthalene-2-carboxylic (pamoic acid) **(A)** and its derivatives including bis-gadolinium-N,N′-bis(diethylenetriamine pentaacetic acid)-pamoic acid bis-hydrazide (bis-Gd-bis-DTPA-pamoate) **(B)**; technetium-99m-tricarbonyl-N-(5-aminopentyl) pyridin-2-yl-methylamino] acetato-4,4′-methylene-2-hydroxy-3 napthalenecarboxamide-(2′-hydroxy-3′ -naphthoic acid methyl ester) (Tc^{99m} $(CO)_3$-pamoate derivative) **(C)**; technetium-99m-tricarbonyl-NN′- bis(diethylenetriamino-pentaacetato)-4,4′-methylene bis(2-hydroxy-3-naphthoic hydrazide (Tc^{99m} $(CO)_3$-bis-DTPA-pamoate) **(D)**; gallium-68-N,N′-bis(diethylenetriamine pentaacetic acid)-pamoic acid bis-hydrazide ([^{68}Ga]-bis-DTPA-pamoate) **(E)**; gallium-68-N,N′-bis(1,4,7,10-tetraazacyclododecane-1,4,7,10-tetraacetic acid)-4,4′-methylene-bis(2-hydroxy-3-naphthoic hydrazide) ([^{68}Ga]-bis-DOTA-pamoate) **(F)**.

About 20 million new cancer cases [83] and a mortality of 12 million deaths [84] have been estimated within the upcoming two decades. Accordingly, rising costs for diagnosis, treatment and follow-up are expected. While surgical removal benefits few patients, radio- and chemo-therapies are commonly regarded as palliative procedures to delay tumor growth and extend patient survival. The development of more innovative and cost-effective strategies is essential to improve cancer management.

Systemic targeted radiotherapy (STR) is an evolving modality that uses systemically administered radioactive agents to preferentially deliver alpha or beta radiation doses to cancer cells while sparing normal tissues. As clinical therapeutic agents, radioiodine for thyroid cancer [85]; metaiodobenzylguanidine labeled to iodine-131 (^{131}I) in the treatment of adrenal medullae tumors [86]; glass radioactive microspheres containing yttrium-90 (^{90}Y) for targeted liver cancer therapy [87]; rhenium-186-1, 1-hydroxyethylidenediphosphonate (^{186}Re-HEDP), strontium-89 chloride (Metastron) and Samarium-153 ethylene diamine tetramethylene phosphonate (^{153}Sm- EDTMP, lexidronam) to relieve pain in patients suffering bone metastases [88, 89] have been used. Anti-CD20 monoclonal antibody (MoAb) labeled with either ^{131}I (tositumomab, Bexxar®) [90] or ^{90}Y (ibritumomab tiuxetan, Zevalin®) [91] for refractory/resistant B-cell non-Hodgkin lymphomas as well as lutetium-177 or ^{90}Y-labeled somatostatin analogs for treating neuroendocrine tumors [92, 93] were also introduced. More recently, radium-223 chloride (^{223}Ra; Alpharadin) was developed for castration-resistant prostate cancer patients with metastatic bone disease [94]. However, few advances have been made to treat the most common solid tumors that feature diverse histological patterns, disorganized angiogenesis [95] and frequent resistance to biology-based therapies due to unpredictable inherent mutations or escaping via overlapped molecular pathways [96, 97].

4.1.1. Tumor Necrosis Treatment (TNT)

Pursuing to evade inherent mutations and escape mechanisms of cancer cells [96], tumor necrosis treatment (TNT) emerged as an innovative anticancer approach that targets the necrotic portion of the tumor [98]. As the proportion of dead cells in tumors can account for above 50% of the total cancer cell population [99], TNT uses MoAb linked to appropriate radionuclides [100] or immune activators [101] that specifically targets intracellular antigens (DNA-histone complex) present in the necrotic tumor areas but absent in living tissues. Thence, they kill nearby remnant tumor cells via radiation cross-fire effect or by generating antitumor immune responses.

The first TNT antibody developed was a murine TNT-1 having specificity for DNA-histone 1 complex that showed to concentrate specifically to tumor necrotic sites in preclinical and clinical studies [102, 103]. In a breakthrough

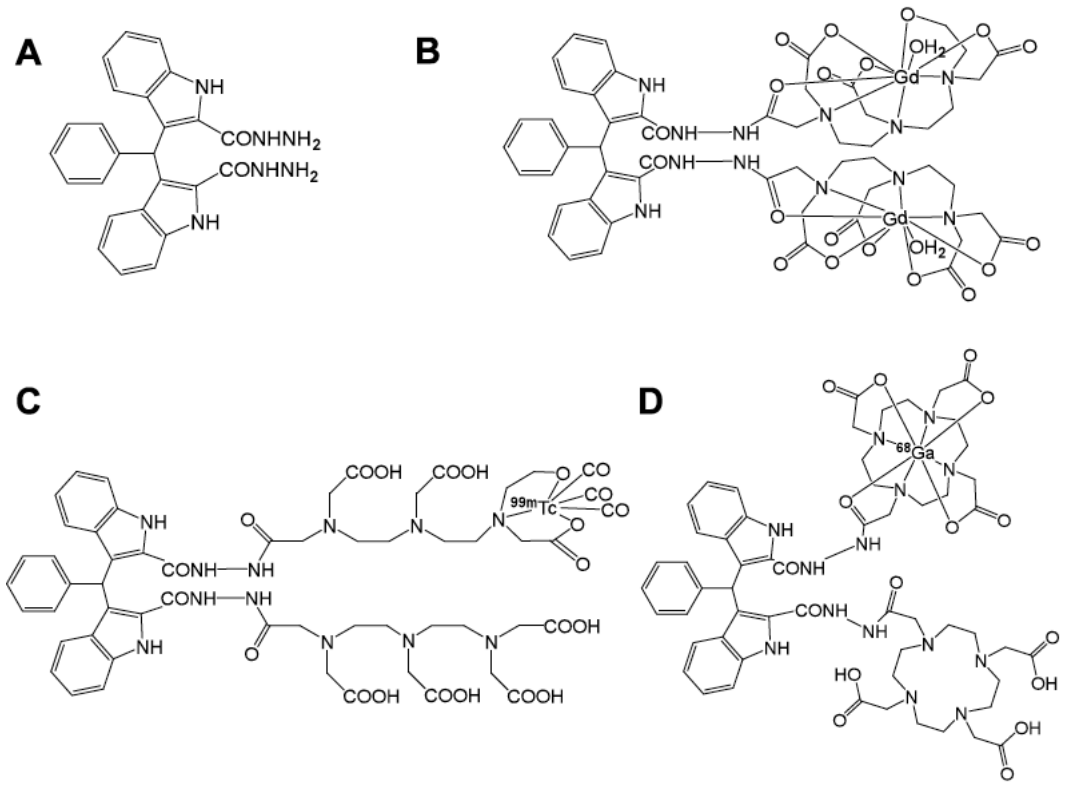

Fig. (9). Chemical structures of 3,3′-(benzylidene)-bis-(1H-indole-2-carbohydrazide) **(A)** and its derivatives including bis-gadollinium-N,N′-bis(diethylenetriamine pentaacetic acid)-3,3′-(benzylidene)-bis-(1H-indole-2-carbohydrazide) (bis-Gd-bis-DTPA-bis-indole) **(B)**; technetium-99m-tricarbonyl- N,N′-bis(diethylenetriamine pentaacetic acid)-3,3′-(benzylidene)-bis-(1H-indole-2-carbohydrazide) ($Tc^{99m}(CO)_3$-bis-DTPA-bis-indole) **(C)**; gallium-68-N,N′-bis(1,4,7,10-tetraazacyclododecane-1,4,7,10-tetraacetic acid)- 3,3′-(benzylidene)-bis-(1H-indole-2-carbohydrazide) ([^{68}Ga]-bis-DOTA-bis-indole **(D)**.

study, Chen *et al.* [102] demonstrated the effective and preferential targeting of TNT-1 MoAb labeled with iodine-131 in nude mice bearing ME-180 human cervical carcinoma. This established the potential clinical usefulness of TNT for imaging and therapeutic treatment of cancer. Three chimeric TNT MoAbs were further developed including chTNT-1, chTNT-2, and chTNT-3 which target histone DNA complexes, heterochromatic DNA, and single-stranded DNA, respectively [104, 105]. Henceforth, over 200 patients have received TNT throughout the world. In a phase I study for advanced colon cancer, the administration of ^{131}I-chTNT-1/B MoAb was well tolerated and without evidence of any significant non-hematologic side effects, however, none of the patients displayed a complete or partial response [106]. Promising therapeutic responses were observed, however, in different clinical trials on patients either with high-grade adult gliomas or advanced lung cancer having received regional administration of ^{131}I-chTNT-1/B MoAb [102, 107]. In a further step, indium-111 labeled genetically engineered Fab' and F(ab')$_2$ constructs of chTNT-3 were evaluated in tumor-bearing mice showing faster clearance from body, improved tissue distribution but lower tumor accumulation than the intact ^{111}In-labeled chTNT-3 MoAb [108].

Further different strategies were applied in order to improve the potentialities of the TNT strategy. Necrosis inducing treatments (NITs) as starting complementary techniques were used for increasing the amount of TNT MoAb binding-necrotic sites on the tumor [109]. Another approach was the synthesis and preclinical evaluation of biotinylated MoAbs with faster whole body clearance times and better biodistribution making them promising candidates for the imaging and therapy of cancer [110]. By means of genetic engineering, TNT-3 antibody was also conjugated to immune activators such as cytokines, or costimulatory molecules leading to fused proteins with superior tumor targeting and immunotherapic potential due to the resulting immune reaction in the tumor surroundings [102]. In a more recent study, a murine TNT-3/CD137L fusion protein was generated, characterized and evaluated in a Colon 26 tumor model. This molecule was able to induce significant tumor suppression by inducing CD8+ T-cell–dependent antitumor responses, which seems to be a useful choice for future clinical trials [111].

However, substantial progresses of TNT-based modality in the clinical practice are far from being achieved. Myelosuppression as the main side effect associated to unfavorable pharmacokinetic properties of radiolabelled MoAbs is continuously observed [106].

4.1.2. OncoCiDia

OncoCiDia is a broad-spectrum anticancer approach with great potential for treating solid malignancies. It refers to a small molecule sequential dual-targeting theragnostic strategy (SMSDTT) [16] based on a "soil-to-seeds" principle that simultaneously allows cancer treatment and diagnostic imaging [17]. Rather than using radiolabeled MoAb with large molecular weight (150 000 g mol^{-1}) and unfavorable pharmacokinetics, OncoCiDia uses two small compounds (<1 000 g mol^{-1}) with complementary targetability and synergetic tumoricidal efficacy.

Initially, a vascular disrupting agent (VDA) is given to selectively destroy established tumor blood vessels leading to intratumoral vascular shutdown and subsequent central necrosis. However, a narrow rim of tumor cells always survives and acts as a germ for tumor repopulation or re-growth [18]. Iodine-131 labeled hypericin is then IV administered to preferentially concentrate at the freshly produced necrotic portion in the tumor, and from there, to eradicate remaining tumor cells via radiation crossfire effect (Fig. **6**) [16, 17]. Because, mono-[^{131}I]iodohypericin has a small molecular size it is able to penetrate faster into tissues and reach less accessible areas across the solid tumor. This may solve previous limitations confronted with the systemic delivery of large sized MoAbs that generally show poor diffusion and distribution through the tumor interstitial space [112].

4.1.2.1. Vascular Disrupting Agents (VDAs)

Vascular disrupting agents (VDAs) are a group of targeted anticancer agents that have been known to synergistically improve radiation, chemotherapy or thermal treatments of solid malignancies. It is well known that intact and functioning blood vessels are essential for cancer cell growth and survival. It has been also reported that blood vasculature in tumors proliferate more rapidly than those in normal tissues [17]. VDAs selectively affect established but fragile vascular network of large solid tumors to trigger vascular shutdown by rapidly destroying tubulin cytoskeleton in the endothelium. Newly formed endothelial cells are more sensitive than mature ones that own well developed actin cytoskeleton and may retain the cell shape in spite of depolymerization of the tubulin cytoskeleton by the VDAs [113]. After VDA administration, the occlusion of blood vessels and capillary sprouts obstructs oxygen and nutrient supply to the tumor cells, compromising cellular integrity and eventually leading to widespread hemorrhagic necrosis at the tumor core [114].

Two main classes of VDAs have been developed including tubulin-binding agents (TBAs) and flavonoids. TBAs cause microtubule depolymerization by binding either the β-subunit of endothelial tubulin of colchicine sites or by disrupting the VE-cadherin/β-catenin complex which interfere with cell–cell contact [115]. Flavonoids derivatives, instead, do not accumulate in tumor-related vasculature, but selectively obstruct blood vessels due to their pharmacodynamics effect such as platelet release due to flavonoid associated-DNA damage to endothelial cells [116]. VDAs can be obtained from natural products such as combretastatins (CA4P, OXi-4503, and AVE-8062), colchicines (ZD6126) and phenylahistin (NPI-2358), whilst others are synthetic compounds (DMXAA, MN-029 and EPC2407) [114].

However the toxicity of VDAs has prevented their usefulness in the clinical setting. So far VDAs with lower toxic effects have been recently developed by conjugating them to other molecules such as polyethylene glycol, CNGRCG peptide or nanoparticles (liposomes, gold) [117]. Regarding treatment efficacy, VDAs have shown limited effectiveness in achieving prolonged antitumor effects [118]. This has been partially related to a 'vascular rebound effect' in which the rims of tumours are more treatment resistant, and can serve as a seed for revascularization and re-population. Therefore, the anticancer effect of VDAs might be enhanced by their combination with other therapeutic modalities such

as radiotherapy, antioangiogenic therapy or chemotherapy [119, 120]. In case of OncoCiDia in which necrosis act as a magnet that attracts the radioactive drugs towards the tumor, alternative necrosis inducing treatments (NITs) can be used mainly in small tumors (< 5 mm), which receive oxygen and nutrients by diffusion from the adjacent tissue [121].

4.1.2.2. Alternative Necrosis Inducing Treatment (NIT) for OncoCiDia

NITs have been developed for treating oncologic patients with tumor recurrences or those who cannot endure conventional surgical resection. NITs are designed to destroy malignant tissues with a minor damage to adjacent normal tissues. Low cost, reduced morbidity and outpatient utilization make them as attractive therapeutic modalities.

Radiofrequency ablation (RFA) causes cell death using heat generated from the high frequency alternating current in the radio-frequency range (460-500 kHz). The ionic agitation in the adjacent tissue produces frictional heat that spreads outwardly from the electrode by conduction [122]. Microwave ablation (MWA) makes use of microwaves to induce an ultra-high-speed (2450 MHz) alternating electric field, which causes the rotation of water molecules [123]. Unlike RFA, MWA does not contain retractable prongs and does not need a ground pad [124]. Laser interstitial thermotherapy (LITT) often applies a neodymium yttrium aluminum garnet (Nd-YAG) laser to deliver high-energy light to the target lesion. Once the light is spread within the tissue, it is converted into heat energy [124]. Unlike RFA, MWA and LITT, cryoablation delivers subfreezing temperatures using probes through which a cryogen is circulated [124]. Percutaneous ethanol injection (PEI) is the simplest, costless technique and requires minimal equipment. By injecting absolute alcohol through a percutaneously placed needle directly into a tumor, cellular dehydration and tissue ischemia from vascular thrombosis occur [125], resulting in chemically induced tumor coagulation necrosis.

4.1.2.3. Iodine-131 Labeled Hypericin (mono-[^{131}I]iodohypericin)

Iodine-131 labeled hypericin (mono-[^{131}I]iodohypericin) can be obtained by electrophilic substitution of iodine-131 (^{131}I) onto the necrosis avid hypericin using mild oxidants such as 1,3,4,6-tetrachloro- 3α, 6α -diphenyl glycoluril (Iodogen) [126]. It is a simple and rapid (< 30 min) method, in which one of the hydrogen atoms on the hydroxyl, aromatic ring of hypericin is substituted with an in situ formed, positively charged ^{131}I atom. Since ^{131}I-Hyp can be produced with high labeling efficiency (> 95%), it can be directly used *in vivo* without further purification steps [127].

In particular, the radionuclide ^{131}I is used as an ionizing radiation source due to its proper physical properties. It is a beta-emitter that has been commonly exploited for treating thyroid cancer due to its native affinity to thyroid tissues as well as relatively easy availability and low cost. Because its mode of radioactive decay with a half-life of 8.02 days and a maximum beta energy of 606 keV (abundance: 89.6%), ^{131}I radiation produces DNA damage and death of cancer cells containing it (self-dose effect) or being at a distance of some millimeters (crossfire effect). Indeed, its tissue penetration of 0.6-2.0 mm [128] allows to radioactively annihilate the residual viable tumor rim, left after CA4P treatment, which typically has a thickness < 100 μm, being well within the irradiation range of the beta particles [58].

In preclinical studies, mono-[^{131}I]iodohypericin has repetitively exhibited high avidity for and long-term retention in necrotic tissues (Fig. **5**) as well as favorable safety profiles *in vivo* [129, 130]. In radionuclide dosimetry studies, mono-[^{131}I]iodohypericin has shown uniquely high absorbed radiation doses in necrotic tumor [131], which appeared to be superior by far to the values reported for other radiotherapeutic agents commercially available or under preclinical investigations [102, 132, 133]. Moreover, since OncoCiDia proposes a sequential administration of two compounds with high, different but complementary targetability, special attentions were also given to evaluate the role of the combination of the VDA treatment and mono-[^{131}I]iodohypericin administration. Overall, tumor eradication was not achieved by injecting either VDA or ^{131}I-hypericin alone. This might be explained by the rapid repopulation of the remaining tumor cells after a single attack with VDA alone. Or with mono-[^{131}I]iodohypericin alone, it might be due to the lack of enough necrotic tumor sites as targeting platform for achieving high concentrations of mono-[^{131}I]iodohypericin whose radiation eventually induces the tumor cell death. It could explain the encouraging therapeutic effects observed after a single treatment with OncoCiDia. In fact, either noticeable shrinkage and significant growth delay in tumor or prolonged survival have been reported in rodents with different allograft tumors being previously treated by the synergetic combination of CA4P and mono-[^{131}I]iodohypericin [16, 58, 134]. Based on these experimental results, this dual-targeting approach appears to be a simple and feasible solution for cancer therapy.

4.1.2.4. Iodine-131 Labeled Sennidin A (monoiodo[^{131}I]-sennindin A)

Because hypericin and its radioiodinated derivatives show poor water solubility leading to the formation of aggregates [135], which are sequestered into the lung macrophages reducing the accumulation of the radiotherapeutic in the necrotic tumor and then impairing its therapeutic effects [129, 136], new alternatives have been explored. Ji *et al.* [137] reported that a radioiodinated derivative of sennidin A, a naturally occurring product originally from the Cassia L. Senna plant, could be a good candidate for OncoCiDia [138]. Although sennidin A has a similar skeleton to hypericin with a condensation of two molecules of anthraquinone, it has more free rotation around the single connecting bond between anthraquinone units. This might allow the sennidin A adopts a spatial arrangement for preventing steric hindrance [137]. This feature could have an important impact on the water solubility of the molecule reducing the formation of aggregations *in vivo* [137] (Fig. **10**). Studies on biodistribution and therapeutic effects of ^{131}I-sennindin A were conducted on S180 tumor-bearing mice prior treated with CA4P to cause tumor necrosis. Results revealed high accumulation and persistent retention of the radioiodinated compound in necrotic tumors and rapid clearance from most normal organs. Synergetic tumoricidal effects such as tumor growth inhibition, prolonged tumor doubling time and extended mean animal survival were consistently observed [137].

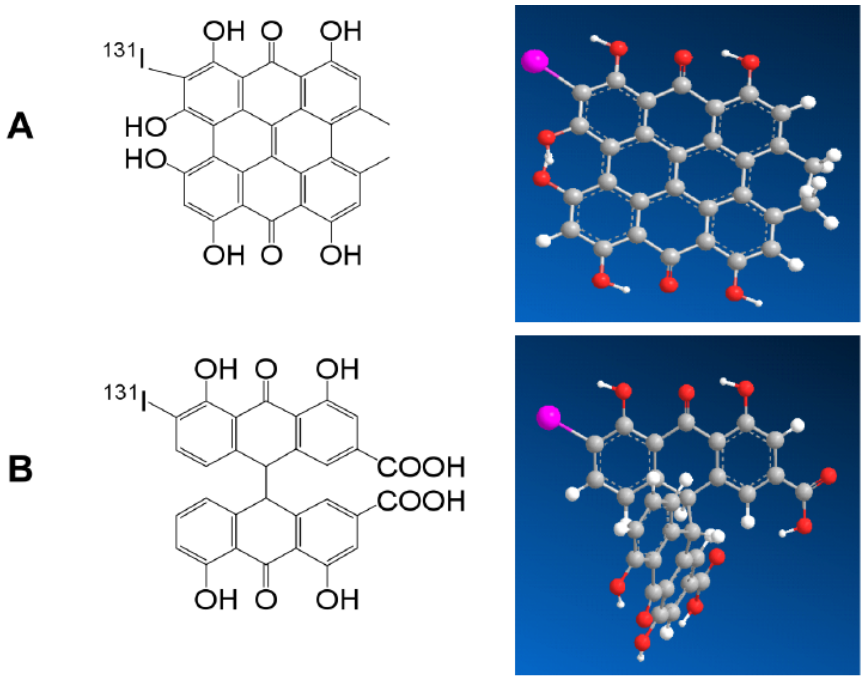

Fig. (10). Bi- and three-dimensional representation of the chemical structures of the mono-[^{131}I]iodohypericin (**A**) and the mono[^{131}I]- iodosennindin A (**B**). Both compounds have similar skeleton characterized by the condensation of two anthraquinone molecules. Contrary to the radioiodinated hypericin, the sennidin A derivative has a single connecting bond between anthraquinone units that allows the molecule to better accommodate in a spatial arrangement for preventing steric effects.

However, contrary to radioiodinated hypericin, the less lipophilic monoiodo[^{131}I]-sennindin A appeared to be highly retained by and excreted through kidneys [137]. This biological profile might lead to acute radiation nephropathy, which has been described as a limiting factor for many other radiotherapeutic agents [139].

5. CONCLUSION

Necrosis is not only a deleterious process in the living body as a response to severe stimuli. Targeting necrosis may offer new opportunities for innumerable diagnosis and treatment applications in diverse diseases. The clinical introduction of necrosis avid agents for optical imaging, magnetic resonance imaging or nuclear imaging may play a complementary role in detection and quantification of acute myocardial infarction and in treatment follow-up. On the other hand, the use of alpha or beta emitter having high affinity for necrotic tissues might play a protagonist role in treating/curing cancer or prolonging the survival of oncologic patients with improved life quality. OncoCiDia is an unconventional but pan-cancer approach based on the necrosis avidity for managing multifocal and multitype malignant tumors. It sequentially uses a vascular disrupting agent for triggering massive tumor necrosis and the necrosis avid iodine-131 labeled hypericin to destroy remaining tumor cells.

LIST OF ABBREVIATIONS

^{11}C	=	Carbon-11
^{18}F	=	Fluorine-18
^{64}Cu	=	Copper-64
^{68}Ga	=	Gallium-68
^{90}Y	=	Yttrium-90
^{99m}Tc	=	Technetium-99m
^{111}In	=	Indium-111
^{123}I	=	Iodine-123
mono-[^{123}I]-iodohypericin	=	Iodine-123 labeled hypericin
^{124}I	=	Iodine-124
^{131}I	=	Iodine-131
mono-[^{131}I]-iodohypericin	=	Iodine-131 labeled hypericin
^{131}I-MIBG	=	Iodine-131 labeled metaiodobenzylguanidine
^{153}Sm-EDTMP	=	Samarium-153 ethylene diamine tetramethylene phosphonate
^{177}Lu	=	Lutetium-177
^{186}Re-HEDP	=	Rhenium-186-1,1-hydroxyethylidenediphosphonate
AVE- 8062	=	Ombrabulin
BMA	=	Gadolinium- diethylene triamine pentaacetic acid- bismethylamide
CA	=	Contrast agent
CA4P	=	Combretastatin A-4 phosphate
CE	=	Contrast enhancement
DMXAA	=	5,6-dimethylxanthenone 4 -acetic acid
DNA	=	Deoxyribonucleic acid

DUR = Duramicyn

Evans Blue = Tetrasodium (6E,6'E)-6,6-[(3,3'-dimethylbiphenyl-4,4'-diyl)di(1E)hydrazin-2-yl-1-ylidene]bis(4-amino-5-oxo-5,6-dihydronaphthalene-1,3-disulfonate

ECIII-60 = bis-gadolinium- diethylene triamine-pentaacetic acid-pamoic acid bis-hydrazide

ECIV-7 = bis- gadolinium- diethylene tria-minepentaacetic acid- benzylidene-bis-indole

EthD-1 = Ethidium homodimer-1

EPC2407 = Crolibulin

Fab = Antibody fragment

FDA = Food and Drug Administration

gadophrin-2 = bis-gadolinium diethylene triamine-pentaacetic acid-mesoporphyrin

Gd = Gadolinium

Gd-DTPA = Gadolinium-diethylene triamine pen-taacetic acid

Gd-DOTA = Gadolinium-tetraazacyclododecane tetraacetic acid

Gd-EOB-DTPA = Gadolinium-ethoxybenzyl diethylene triamine pentaacetic acid

Gd-BOPTA = Gadobenate dimeglumine

GST = Glutathione S-transferase

hypericin = 1,3,4,6,8,13-hexahydroxy-10,11-dimethylphenanthro[1,10,9,8-opqra]perylene-7,14-dione

HYNIC = 6-hydrazinopyridine-3-carboxylic acid

Iodogen = 1,3,4,6-tetrachloro-3α,6α-diphenyl glycoluril

IFNs = Interferons

IV = Intravenous

Kd = Dissociation constant

LDL = Low-density lipoprotein

LITT = Laser interstitial thermotherapy

MI = Myocardial infarction

MLKL = Mixed lineage kinase domain-like protein

Mn = Manganese

MN-029 = Denibulin di-hydrochloride

Mn-DPDP = Dipyridoxyl diphosphate

MoAb = Monoclonal antibody

MPT = Mitochondrial permeability transi-tion

MRI = Magnetic resonance imaging

MW = Molecular weight

MWA = Microwave ablation

NAC = Necrosis avid compounds

NACA = Necrosis avid contrast agents

NADPH = Nicotinamide adenine dinucleotide phosphate-oxidase

NIT = Necrosis inducing treatment

NPI-2358 = Plinabulin

NSCLC = Non-small-cell lung carcinoma

OI = Optical imaging

OXi-4503 = Combretastatin A1 di-phosphate / CA1P

PARP1 = Poly (adenosine diphosphate-ribose) polymerase 1

PAMPs = Pathogen-associated molecular pat-terns

PE = Phosphatidylethanolamine

PEG400 = Polyethylene glycol 400

PEI = Percutaneous ethanol injection

PI = Propidium iodide

PTA = Photothermal ablation

PS = Phosphatidylserine

R1 = Rhabdomyosarcoma

RFA = Radiofrequency ablation

RLRs = Retinoic acid inducible gene I (RIG-I)-like receptors

RIP1/3 = Receptor-interacting protein-1/3

RIF-1 = Radiation-induced fibrosarcoma

RPLI = Reperfused partial liver infarction

SMSDTT = Small molecule sequential dual-targeting theragnostic strategy

SPECT = Single photon emission computed tomography

STR = Systemic targeted radiotherapy

TBA = Tubulin binding agents

3D-OCT = Three-dimensional optical coherence tomography

TNF = Tumor-necrosis factor

T1 = T1 relaxation time or spin-lattice relaxation time

T2 = T2 relaxation time

TTC = 2,3,5-Triphenyl-2H-tetrazolium chloride

TNT = Tumor necrosis treatment

TLR4	=	Toll-like receptor 4
TRAIL	=	Tumor necrosis factor -related apoptosis-inducing ligand
TWEAK	=	Tumor necrosis factor -related weak inducer of apoptosis
VDA	=	Vascular disrupting agent
ZD6126	=	N-Acetylcolchicinol dihydrogen-phosphate

CONFLICT OF INTEREST

The authors confirm that this article content has no conflict of interest.

ACKNOWLEDGEMENTS

This study has been supported in part by Research Foundation – Flanders (FWO), the K.U. Leuven Molecular Small Animal Imaging Center MoSAIC (KUL EF/05/08); the center of excellence *in vivo* molecular imaging research of K.U. Leuven; KU Leuven project IOF-HB/08/009; and the European Union (Asia-Link CfP 2006-EuropeAid/123738/C/ ACT/Multi-Proposal No. 128 – 498/111).

REFERENCES

[1] Kitanaka, C.; Kuchino, Y. Caspase-independent programmed cell death with necrotic morphology. *Cell. Death Differ.,* **1999**, *6* (6), 508-515.

[2] Kumar, V.; Abbas, A. K.; Aster, J. C. Causes of cell injury. In: Robbins. Basic Pathology, 9 ed. Elsevier Saunders: USA, **2013**; pp. 1-26.

[3] Ni, Y.; Bormans, G.; Chen, F.; Verbruggen, A.; Marchal, G. Necrosis avid contrast agents functional similarity versus structural diversity. *Invest. Radiol.,* **2005**, *40* (8), 526-35.

[4] Ni, Y.; Cresens, E.; Adriaens, P.; Miao, Y.; Verbeke, K.; Dymarkowski, S.; Verbruggen, A.; Marchal, G. Necrosis-avid contrast agents: introducing nonporphyrin species. *Acad. Radiol.,* **2002**, *9* (1), S98-S101.

[5] Ni, Y.; Marchal, G.; Jie, Y.; Lukito, G.; Petré, C.; Wevers, M.; Baert, A. L.; Ebert, W.; Hilger, C. S.; Maier, F. K. Localization of metalloporphyrin-induced "specific" enhancement in experimental liver tumors: comparison of magnetic resonance imaging, microangiographic, and histologic findings. *Acad. Radiol.,* **1995**, *2* (8), 687-699.

[6] Cresens, E.; Ni, Y.; Adriaens, P.; Verbruggen, A.; Marchal, G. Substituted bis-indole derivatives useful as contrast agents, pharmaceutical compositions containing them and intermediates for producing them. EP 1343758 A1, 2003.

[7] Ell, P. J.; Langford, R.; Pearce, P.; Lui, D.; Elliott, A. T.; Woolf, N.; Williams, E. S. ^{99m}Tc-imidodiphosphonate: a superior radiopharmaceutical for *in. vivo* positive myocardial infarct imaging. I: Experimental data. *Br. Heart J.,* **1978**, *40* (3), 226-233.

[8] Obrador, D.; Ballester, M.; Carrió, I.; Augé, J. M.; López, C. M.; Bosch, I.; Martí, V.; Bordes, R. Active myocardial damage without attending inflammatory response in dilated cardiomyopathy. *J. Am. Coll. Cardiol.,* **1993**, *21*(7), 1667-1671.

[9] Dec, G. W.; Palacios, I.; Yasuda, T.; Fallon, J.T.; Khaw, B. A.; Strauss, H. W.; Haber, E. Antimyosin antibody cardiac imaging: its role in the diagnosis of myocarditis. *J. Am. Coll. Cardiol.,* **1990**, *16* (1), 97-104.

[10] Frist, W.; Yasuda, T.; Segall, G.; Khaw, B. A.; Strauss, H. W.; Gold, H.; Stinson, E.; Oyer, P.; Baldwin, J.; Billingham, M. Noninvasive detection of human cardiac transplant rejection with indium-111 antimyosin (Fab) imaging. *Circulation.,* **1987**, *76* (5 Pt 2), V81-85.

[11] Jiang, C.; Li, Y.; Jiang, X.; Yao, N.; Gao, M.; Zhang, X.; Wang, J.; Wang, X.; Sun, Z.; Zhang, J.; Ni, Y. Hypericin as a marker for determination of myocardial viability in a rat model of myocardial infarction. *Photochem. Photobiol.,* **2014**, 90, 867-872.

[12] Buja, L. M.; Tofe, A. J.; Kulkarni, P. V.; Mukherjee, A.; Parkey, R. W.; Francis, M. D.; Bonte, F. J.; Willerson, J. T. Sites and mechanisms of localization of technetium-99m phosphorus radiopharmaceuticals in acute myocardial infarcts and other tissues. *J. Clin. Invest.,* **1977**, *60* (3), 724-740.

[13] Khaw, B. A.; Nakazawa, A.; O'Donnell, S. M.; Pak, K. Y.; Narula, J. Avidity of technetium 99m glucarate for the necrotic myocardium: *in vivo* and *in vitro* assessment. *J. Nucl. Cardiol.,* **1997**, *4*(4), 283-290.

[14] Hiroe, M.; Ohta, Y.; Fujita, N.; Nagata, M.; Toyozaki, T.; Kusakabe, K.; Sekiguchi, M.; Marumo, F. Myocardial uptake of ^{111}In monoclonal antimyosin Fab in detecting doxorubicin cardiotoxicity in rats. Morphological and hemodynamic findings. *Circulation.,* **1992**, *86* (6), 1965-1972.

[15] Ni, Y.; Huyghe, D.; Verbeke, K.; de Witte, P. A.; Nuyts, J.; Mortelmans, L.; Chen, F.; Marchal, G.; Verbruggen, A.; Bormans, G. First preclinical evaluation of mono-[^{123}I]iodohypericin as a necrosis-avid tracer agent. *Eur. J. Nucl. Med. Mol. Imaging,* **2006**, *33* (5), 595-601.

[16] Li, J.; Sun, Z.; Zhang, J.; Shao, H.; Cona, M. M.; Wang, H.; Marysael, T.; Chen, F.; Prinsen, K.; Zhou, L.; Huang, D.; Nuyts, J.; Yu, J.; Meng, B.; Bormans, G.; Fang, Z.; de Witte, P.; Li, Y.; Verbruggen, A.; Wang, X.; Mortelmans, L.; Xu, K.; Marchal, G.; Ni, Y. A dual-targeting anticancer approach: soil and seed principle, *Radiology,* **2011**, *260* (3): 799-807.

[17] Katholieke Universiteit Leuven – Oncocidia. Available from: http://vimeo.com/44871398 (accessed August 8*.,* 2014).

[18] Tozer, G. M.; Kanthou, C.; Baguley, B. C. Disrupting tumor blood vessels. *Nat. Rev. Cancer,* **2005**, *5*(6), 423-435.

[19] Stefanis, L. Caspase-dependent and -independent neuronal death: two distinct pathways to neuronal injury. *Neuroscientist,* **2005**, *11* (1), 50-62.

[20] Kroemer, G.; Galluzzi, L.; Vandenabeele, P.; Abrams, J.; Alnemri, E. S.; Baehrecke, E. H.; Blagosklonny, M. V.; El-Deiry, W. S.; Golstein, P.; Green, D. R.; Hengartner, M.; Knight, R. A.; Kumar, S.; Lipton, S. A.; Malorni, W.; Nuñez, G.; Peter, M. E.; Tschopp, J.; Yuan, J.; Piacentini, M.; Zhivotovsky, B.; Melino, G. Classification of cell death: recommendations of the nomenclature committee on cell death 2009. *Cell. Death Differ.,* **2009**, *16* (1), 3-11.

[21] Degterev, A.; Hitomi, J.; Germscheid, M.; Chen, I. L.; Korkina, O.; Teng, X.; Abbot, D.; Cuny, G. D.; Yuan, C.; Wagner, G.; Hedrick, S. M.; Gerber, S. A.; Lugovskoy, A.; Yuan, J. Identification of RIP1 kinase as a specific cellular target of necrostatins. *Nat. Chem. Biol.,* **2008**, *4*, 313-321.

[22] Berghe, T. V.; Linkermann, A.; Jouan-Lanhouet, S.; Walczak, H.; Vandenabeele, P. Regulated necrosis: the expanding network of non-apoptotic cell death pathways. *Nat. Rev. Mol. Cell. Biol.,* **2014**, *15*, 135-147.

[23] Yu, L.; Alva, A.; Su, H.; Dutt, P.; Freundt, E.; Welsh, S.; Baehrecke, E. H.; Lenardo, M. J. Regulation of an ATG7-beclin 1 program of autophagic cell death by caspase-8. *Science,* **2004**, *304* (5676), 1500-1529.

[24] Miao, B.; Degterev, A. Methods to analyze cellular necroptosis. *Methods. Mol. Biol.,* **2009**, *559*, 79-93.

[25] Alvarez, A.; Lacalle, J.; Cañavate, M. L.; Alonso-Alconada, D.; Lara-Celador, I.; Alvarez, F. J.; Hilario, E. Cell death. A comprehensive approximation. Necrosis. In: *Microscopy. Science., Technology., Applications and Education*, Méndez-Vilas, A & Díaz, J., Eds*.,* **2010**; pp 1017-1024.

[26] Ziegler, U.; Groscurth, P. Morphological features of cell death. *Physiology.,* **2004**, *19,* 124-128.

[27] Lewandrowski, K.; Chen, A.; Januzzi, J. Cardiac markers for myocardial infarction. A brief review. *Am. J. Ind. Med.,* **2002**, *118 (Suppl)*, S93-99.

[28] Cevik, U. I.; Dalkara, T. Intravenously administered propidium iodide labels necrotic cells in the intact mouse brain after injury. *Cell. Death Differ.,* **2003**, *10*, 928-929.

[29] Alt, A.; Hilgers, R.D.; Tura, A.; Nassar, K.; Schneider, T.; Hueber, A.; Januschowski, K.; Grisanti, S.; Lüke, J.; Lüke, M. The neuroprotective potential of Rho-kinase inhibition in promoting cell survival and reducing reactive gliosis in response to hypoxia in isolated bovine retina. *Cell. Physiol. Biochem.,* **2013**, *32* (1), 218-234.

[30] Yeo, D.; Kiparissides, A.; Cha, J. M.; Aguilar-Gallardo, C.; Polak, J. M.; Tsiridis, E.; Pistikopoulos, E. N.; Mantalaris, A. Improving embryonic stem cell expansion through the combination of perfu-

sion and bioprocess model design. *PLOS ONE,* **2013**, *8* (12), e81728.

[31] Honda, O.; Kuroda, M.; Joja, I.; Asaumi, J.; Takeda, Y.; Akaki, S.; Togami, I.; Kanazawa, S.; Kawasaki, S.; Hiraki, Y. Assessment of secondary necrosis of Jurkat cells using a new microscopic system and double staining method with annexin V and propidium iodide. *Int. J. Oncol.,* **2000**, *16* (2), 283-288.

[32] Tali® Apoptosis Kit - Annexin V Alexa Fluor® 488 & Propidium Iodide. http://tools.lifetechnologies.com/content/sfs/manuals/mp10788.pdf. Accessed on December 20th, 2014.

[33] Yániz, J. L.; Palacín, I.; Vicente-Fiel, S.; Gosalvez, J.; López-Fernández, C.; Santolaria, P. Comparison of membrane-permeant fluorescent probes for sperm viability assessment in the ram. *Reprod. Domest. Anim.,* **2013**, *48* (4), 598-603.

[34] Andras, S. C.; Hartman, T. P. V.; Alexander, J.; McBride, R.; Marshall, J. A.; Power, J. B.; Cocking, E. C.; Davey, M. R. Combined PI-DAPI staining (CPD) reveals NOR asymmetry and facilitates karyotyping of plant chromosomes. *Chromosome. Res.,* **2000**, *8* (5), 387-391.

[35] World Health Organization. The top 10 causes of death. Fact sheet no. 310 2011. Available from: http://www.who.int/mediacentre/factsheets/fs310/en/index.html. (accessed July 24, 2014).

[36] Finn, A. V.; Nakano, M.; Narula, J.; Kolodgie, F. D.; Virmani, R. Concept of vulnerable/unstable plaque. *Arterioscler. Thromb. Vasc. Biol.,* **2010**, *30*, 1282-1292.

[37] Kim, R. J.; Wu, E.; Rafael, A.; Chen, E. L.; Parker, M. A.; Simonetti, O.; Klocke, F. J.; Bonow, R. O.; Judd, R. M. Contrast-enhanced magnetic resonance imaging to identify reversible myocardial dysfunction. *N. Engl. J. Med.,* **2000**, *343* (20), 1445-1453.

[38] Weinmann, H. J.; Laniado, M.; Mützel, W. Pharmacokinetics of GdDTPA/dimeglumine after intravenous injection into healthy volunteers. *Physiol. Chem. Phys. Med. NMR.,* **1984**, *16* (2), 167-172.

[39] Pereira, R. S.; Prato, F. S.; Wisenberg, G.; Sykes, J.; Yvorchuk, K. J. The use of Gd-DTPA as a marker of myocardial viability in reperfused acute myocardial infarction. *Int. J. Cardiovasc. Imaging,* **2001**, *17* (5), 395-404.

[40] Marckmann, P. Nephrogenic systemic fibrosis: epidemiology update. *Curr. Opin. Nephrol. Hypertens.,* **2008**, *17* (3), 315-319.

[41] Adzamli, I. K.; Blau, M.; Pfeffer, M. A.; Davis, M. A. Phosphonate-modified Gd-DTPA complexes. III: The detection of myocardial infarction by MRI. *Magn. Reson. Med.,* **1993**, *29* (4), 505-511.

[42] Elizondo, G.; Fretz, C. J.; Stark, D. D.; Rocklage, S. M.; Quay, S. C.; Worah, D.; Tsang, Y. M.; Chen, M. C.; Ferrucci, J. T. Preclinical evaluation of Mn-DPDP: new paramagnetic hepatobiliary contrast agent for MR imaging. *Radiology,* **1991**, *178* (1), 73-78.

[43] Schuhmann-Giampieri, G.; Schmitt-Willich, H.; Press, W. R.; Negishi, C.; Weinmann, H. J.; Speck, U. Preclinical evaluation of Gd-EOB-DTPA as a contrast agent in MR imaging of the hepatobiliary system. *Radiology,* **1992**, *183* (1), 59-64.

[44] Vittadini, G.; Felder, E.; Musu, C.; Tirone, P. Preclinical profile of Gd-BOPTA. A liver-specific MRI contrast agent. *Invest. Radiol.,* **1990**, *25(*Suppl 1), S59-60.

[45] Ni, Y.; Bormans, G.; Marchal, G.; Verbruggen, A. Necrosis avid tracer agent. E.P. 1 651 201 B1, January, 2008.

[46] Metz, S.; Daldrup-Unk, H. E.; Richter, T.; Räth, C.; Ebert, W.; Settles, M.; Rummeny, E. J.; Link, T. M.; Piert, M. Detection and quantification of breast tumor necrosis with MR imaging: value of the necrosis-avid contrast agent Gadophrin-3. *Acad. Radiol.,* **2003**, *10* (5), 484-490.

[47] Jørgensen, M. Quantitative determination of pamoic acid in dog and rat serum by automated ion-pair solid-phase extraction and reversed-phase high-performance liquid chromatography. *J. Chromatogr. B. Biomed. Sci. Appl.,* **1998**, *716* (1-2), 315-323.

[48] Shaaban, M.; Maskey, R. P.; Wagner-Döbler, I.; Laatsch, H. Pharacine, a natural p-cyclophane and other indole derivatives from Cytophaga sp. strain AM13.1. *J. Nat. Prod.,* **2002**, *65* (11), 1660-1663.

[49] Chen, B.; Zupkó, I.; de Witte, P. A. Photodynamic therapy with hypericin in a mouse P388 tumor model: vascular effects determine the efficacy. *Int. J. Oncol.,* **2001**, *18* (4), 737-742.

[50] Roth, L., *Hypericum., Hypericin. :. Botanik., Inhaltsstoffe., Wirkung*. Landsberg, Lech: Ecomed **1990**.

[51] Karioti, A.; Bilia, A. R. Hypericins as potential leads for new therapeutics. *Int. J. Mol. Sci.,* **2010**, *11*, 562-594.

[52] Jiang, B.; Wang, J.; Ni, Y.; Chen, F. Necrosis avidity: a newly discovered feature of hypericin and its preclinical applications in necrosis imaging. *Theranostics,* **2013**, *3* (9), 667-676.

[53] Hypericin. Characteristics. In: Encyclopedia of Cancer, 3rd ed.; Schwab, M., Ed. Springer: USA, **2012**; Vol. 1, p. 1781.

[54] Hueper, W. C.; Ichniowski, C. T. Toxicopathologic studies on the dye T-1824. *Arch. Surg.,* **1944**, *48* (1), 17-26.

[55] Rawson, R. A. The binding of T-1824 and structurally related diazo dyes by the plasma proteins. *Am. J. Physiol.,* **1942-43**, *138*, 708-717.

[56] Klyen, B. R.; Shavlakadze, T.; Radley-Crabb, H. G.; Grounds, M. D.; Sampson, D. D. Identification of muscle necrosis in the mdx mouse model of Duchenne muscular dystrophy using three-dimensional optical coherence tomography. *J. Biomed. Opt.,* **2011**, *16* (7), 076013.

[57] Van de Putte, M.; Marysael, T.; Fonge, H.; Roskams, T.; Cona, M. M.; Li, J.; Bormans, G.; Verbruggen, A.; Ni, Y.; de Witte, P. Radiolabeled iodohypericin as tumor necrosis avid tracer: diagnostic and therapeutic potential. *Int. J. Cancer,* **2012**, *131*, E129-E137.

[58] Li, J.; Cona, M. M.; Chen, F.; Feng, Y.; Zhou, L.; Yu, J.; Nuyts, J.; de Witte, P.; Zhang, J.; Himmelreich, U.; Verbruggen, A.; Ni, Y. Exploring theranostic potentials of radioiodinated hypericin in rodent necrosis models. *Theranostics,* **2012**, 2 (10), 1010-1019.

[59] Feng, Y.; Chen, F.; Ma, Z.; Dekeyzer, F.; Yu, J.; Xie, Y.; Cona, M. M.; Oyen, R.; Ni, Y. Towards stratifying ischemic components by cardiac MRI and multifunctional stainings in a rabbit model of myocardial infarction. *Theranostics,* **2013**, *4*(1), 24-35.

[60] Bianco, J. A.; Kemper, A. J.; Taylor, A.; Lazewatsky, J.; Tow, D. E.; Khuri, S. F. Technetium-99m(Sn^{2+}) pyrophosphate in ischemic and infarcted dog myocardium in early stages of acute coronary occlusion: histochemical and tissue-counting comparisons. *J. Nucl. Med.,* **1983**, *24* (6), 485-491.

[61] Khaw, B. A.; Strauss, H. W.; Moore, R.; Fallon, J. T.; Yasuda, T.; Gold, H. K.; Haber, E. Myocardial damage delineated by indium-111 antimyosin Fab and technetium-99m pyrophosphate. *J. Nucl. Med.,* **1987**, *28* (1), 76-82.

[62] Hayashi, F.; Nagashima, K.; Terui, Y.; Kawamura, Y.; Matsumoto, K.; Itazaki, H. The structure of PA48009: the revised structure of duramycin. *J. Antibiot. (Tokyo),* **1990**, *43* (11), 1421-1430.

[63] Zimmermann, N.; Freund, S.; Fredenhagen, A.; Jung, G. Solution structures of the lantibiotics duramycin B and C. *Eur. J. Biochem.,* **1993**, *216* (2), 419-428.

[64] Iwamoto, K.; Hayakawa, T.; Murate, M.; Makino, A.; Ito, K.; Fujisawa, T.; Kobayashi, T. Curvature-dependent recognition of ethanolamine phospholipids by duramycin and cinnamycin. *Biophys. J.,* **2007**, *93* (5), 1608-1619.

[65] Zhao, M.; Li, Z.; Bugenhagen, S. ^{99m}Tc-labeled duramycin as a novel phosphatidylethanolamine-binding molecular probe. *J. Nucl. Med.,* **2008**, *49* (8), 1345-1352.

[66] Bejot, R.; Goggi, J. Development of a duramycin-based PET probe for imaging apoptosis. *J. Nucl. Med.,* **2012**, *53* (Suppl. 1), 1652.

[67] Cona, M. M.; Feng, Y.; Li, Y.; Chen, F.; Vunckx, K.; Zhou, L.; Slambrouck, K. V.; Rezaei, A.; Gheysens, O.; Nuyts, J.; Verbruggen, A.; Oyen, R.; Ni, Y. Comparative study of iodine-123-labeled hypericin and ^{99m}Tc-labeled hexakis [2-methoxy isobutyl isonitrile] in a rabbit model of myocardial infarction. *J. Cardiovasc. Pharmacol.,* **2013**, *62* (3), 304-311.

[68] Fonge, H.; Van de Putte, M.; Huyghe, D.; Bormans, G.; Ni, Y.; de Witte, P.; Verbruggen, A. Evaluation of tumor affinity of mono-[^{123}I]iodohypericin and mono-[^{123}I]iodoprotohypericin in a mouse model with a RIF-1 tumor. *Contrast. Media. Mol. Imaging.* **2007**, *2* (3), 113-119.

[69] Fonge, H.; Jin, L.; Wang, H.; Ni, Y.; Bormans, G.; Verbruggen, A. Synthesis and preliminary evaluation of mono-[^{123}I]iodohypericin monocarboxylic acid as a necrosis avid imaging agent. *Bioorg. Med. Chem. Lett.,* **2007**, *17* (14), 4001-4005.

[70] Fonge, H.; Jin, L.; Wang, H.; Bormans, G.; Ni, Y.; Verbruggen, A. Synthesis and preliminary biological evaluation of a ^{99m}Tc-labeled hypericin derivative as a necrosis avid imaging agent.. *J. Labell. Comp. Radiopharm.,* **2008**, *51* (1), 33-40.

[71] Chopra, A. ^{64}Cu-Labeled bis-1,4,7,10-tetraazacyclododecane-N,N',N,N'-tetraacetic acid conjugated hypericin. *Molecular Imaging and Contrast Agent Database (MICAD),* 2013.

[72] Tsopelas, C.; Bellon, M.; Bevington, E.; Kollias, J.; Shibli, S.; Chatterton, B. E. Lymphatic mapping with ^{99m}Tc-Evans Blue dye in sheep. *Ann. Nucl. Med.,* **2008**, *22* (9), 777-785.

[73] Khaw, B. A.; Strauss, H. W.; Moore, R.; Fallon, J. T.; Yasuda, T.; Gold, H. K.; Haber, E. Myocardial damage delineated by indium-111 antimyosin Fab and technetium-99m pyrophosphate. *J. Nucl. Med.,* **1987**, *28* (1), 76-82.

[74] Taillefer, R.; Boucher, L.; Lambert, R.; Grégoire, J.; Phaneuf, D. C.; Sikorsa, H. Technetium-99m antimyosin antibody (3-48) myocardial imaging: human biodistribution, safety and clinical results in detection of acute myocardial infarction. *Eur. J. Nucl. Med.,* **1995**, *22* (5), 453-464.

[75] Thiagarajan, P.; Tait, J. F. Binding of annexin V/placental anticoagulant protein I to platelets. Evidence for phosphatidylserine exposure in the procoagulant response of activated platelets. *J. Biol. Chem.,* **1990**, *265* (29), 17420-17423.

[76] Belhocine, T. Z.; Prato, F. S. Transbilayer phospholipids molecular imaging. *EJNMMI. Res.,* **2011**, *1*(1), 17.

[77] Zhao, M.; Zhu, X.; Ji, S.; Zhou, J.; Ozker, K. S.; Fang, W.; Molthen, R. C.; Hellman, R. S. ^{99m}Tc-labeled C2A domain of synaptotagmin I as a target-specific molecular probe for noninvasive imaging of acute myocardial infarction. *J. Nucl. Med.,* **2006**, *47* (8), 1367-1374.

[78] Wang, F.; Fang, W.; Zhao, M.; Wang, Z.; Jie, S.; Li, Y.; Zheng, Y. Imaging paclitaxel (chemotherapy)-induced tumor apoptosis with ^{99m}Tc C2A, a domain of synaptotagmin I: a preliminary study. *Nucl. Med. Biol.,* **2008**, *35* (3), 359-364.

[79] Wang, F.; Fang, W.; Zhang, M. R.; Zhao, M.; Liu, B.; Wang, Z.; Hua, Z.; Yang, M.; Kumata, K.; Hatori, A.; Yamasaki, T.; Yanamoto, K.; Suzuki, K. Evaluation of chemotherapy response in VX2 rabbit lung cancer with ^{18}F-labeled C2A domain of synaptotagmin I. *J. Nucl. Med.,* **2011**, *52* (4), 592-599.

[80] Fonge, H.; Chitneni, S. K.; Lixin, J.; Vunckx, K.; Prinsen, K.; Nuyts, J.; Mortelmans, L.; Bormans, G.; Ni, Y.; Verbruggen, A. Necrosis avidity of ^{99m}Tc(CO)$_3$-labeled pamoic acid derivatives: synthesis and preliminary biological evaluation in animal models of necrosis. *Bioconjug. Chem.,* **2007**, *18* (6), 1924-1934.

[81] Prinsen, K.; Li, J.; Vanbilloen, H.; Vermaelen, P.; Devos, E.; Mortelmans, L.; Bormans, G.; Ni, Y.; Verbruggen, A. Development and evaluation of a ^{68}Ga labeled pamoic acid derivative for *in. vivo* visualization of necrosis using positron emission tomography. *Bioorg. Med. Chem.,* **2010**, *18* (14), 5274-5281.

[82] Prinsen, K.; Cona, M. M.; Cleynhens, J.; Vanbilloen, H.; Li, J.; Dyubankova, N.; Lescrinier, E.; Bormans, G.; Ni, Y.; Verbruggen, A. Synthesis and biological evaluation of ^{68}Ga labeled bis-DOTA-3,3′-(benzylidene)-bis-(^{1}H-indole-2-carbohydrazide) as a PET tracer for *in. vivo* visualization of necrosis. *Bioorg. Med. Chem. Lett.,* **2013**, *23* (11), 3216-3220.

[83] Cancer American Society. Global Cancer Facts & Figures. http://www.cancer.org/research/cancerfactsstatistics/global (accessed July 16*.,* 2014).

[84] Bray, F.; Møller, B. Predicting the future burden of cancer. *Nat. Rev. Cancer,* **2006,** *6*, 63-74.

[85] Luster, M.; Clarke, S. E.; Dietlein, M.; Lassmann, M.; Lind, P.; Oyen, W. J.; Tennvall, J.; Bombardieri, E. Guidelines for radioiodine therapy of differentiated thyroid cancer. *Eur. J. Nucl. Med. Mol. Imaging.,* **2008**, *35* (10), 1941-1959.

[86] Taşdelen, B.; Kam, E.; Asliyuksek, H. Quality control of iodine-131-labeled metaiodobenzylguanidine. *Nucl. Med. Commun.,* **2014**, *35* (1), 95-98.

[87] Rhee, T. K.; Lewandowski, R. J.; Liu, D. M.; Mulcahy, M. F.; Takahashi, G.; Hansen, P. D.; Benson, A. B. 3rd.; Kennedy, A. S.; Omary, R. A.; Salem, R. ^{90}Y Radioembolization for metastatic neuroendocrine liver tumors: preliminary results from a multi-institutional experience. *Ann. Surg.,* **2008**, *247* (6), 1029-1035.

[88] Sideras, P. A.; Stavraka, A.; Gouliamos, A.; Limouris, G. S. Radionuclide therapy of painful bone metastases--a comparative study between consecutive radionuclide infusions, combination with chemotherapy, and radionuclide infusions alone: an *in vivo* comparison of their effectiveness. *Am. J. Hosp. Palliat. Care.,* **2013**, *30* (8), 745-751.

[89] Sartor, O. Overview of samarium Sm-153 Lexidronam in the treatment of painful metastatic bone disease. *Rev. Urol.,* **2004**, *6* (Suppl 10), S3-S12.

[90] Smith, K.; Byer, G.; Morris, C. G.; Kirwan, J. M.; Lightsey, J.; Mendenhall, N. P.; Hoppe, B. S.; Lynch, J.; Olivier, K. Outcomes of patients with non-hodgkin's lymphoma treated with bexxar with or without external-beam radiotherapy. *Int. J. Radiat. Oncol. Biol. Phys.,* **2012**, *82* (3), 1122-1127.

[91] Micallef, I. N. Ongoing trials with yttrium 90-labeled ibritumomab tiuxetan in patients with non-Hodgkin's lymphoma. *Clin. Lymphoma.,* **2004**, *5* (Suppl 1), S27-32.

[92] Virgolini, I.; Traub, T.; Novotny, C.; Leimer, M.; Fuger, B.; Li, S. R.; Patri, P.; Pangerl, T.; Angelberger, P.; Raderer, M.; Burggasser, G.; Andreae, F.; Kurtaran, A.; Dudczak, R. Experience with indium-111 and yttrium-90-labeled somatostatin analogs. *Curr. Pharm. Des.,* **2002**, *8* (20), 1781-1807.

[93] Kwekkeboom, D. J.; Kam, B. L.; van Essen, M.; Teunissen, J. J.; van Eijck, C. H.; Valkema, R.; de Jong, M.; de Herder, W. W.; Krenning, E. P. Somatostatin receptor-based imaging and therapy of gastroenteropancreatic neuroendocrine tumors. *Endocr. Relat. Cancer,* **2010**, *17* (1), R53-73.

[94] Harrison, M. R.; Wong, T. Z.; Armstrong, A. J.; George, D. J. Radium-223 chloride: a potential new treatment for castration-resistant prostate cancer patients with metastatic bone disease. *Cancer Manag. Res.,* **2013**, *5*, 1-14.

[95] Jarm, T.; Cemazar, M.; Miklavcic, D.; Sersa, G. Antivascular effects of electrochemotherapy: implications in treatment of bleeding metastases. *Expert. Rev. AntiCancer Ther.,* **2010**, *10* (5), 729-746.

[96] Merlo, L. M. F.; Pepper, J. W.; Reid, B. J.; Maley, C. C. Cancer as an evolutionary and ecological process. *Nat. Rev. Cancer,* **2006**, *6*(12), 924-935.

[97] Nowell, P. C. The clonal evolution of tumor cell populations. *Science.,* **1976**, *194* (4260), 23-28.

[98] Epstein, A. L.; Chen, F. M.; Taylor, C. R. A novel method for the detection of necrotic lesions in human cancers. *Cancer Res.,* **1988**, *48* (20), 5842-5848.

[99] Malaise, E. P.; Chavaudra, N.; Tubiana, M. The relationship between growth rate, labeling index and histological type of human solid tumors. *Eur. J. Cancer,* **1973**, *9* (4), 305-312.

[100] Chen, F. M.; Taylor, C. R.; Epstein, A. L. Tumor necrosis treatment of ME-180 human cervical carcinoma model with ^{131}I-labeled TNT-1 monoclonal antibody. *Cancer Res.,* **1989**, *49* (16), 4578-4585.

[101] Khawli, L. A.; Hu, P.; Epstein, A. L. Cytokine, chemokine, and costimulatory fusion proteins for the immunotherapy of solid tumors. In: *Therapeutic Antibodies* Chernajovsky, Y.; Ahuva, N.; Eds. Springer: Berlin Heidelberg **2008**; Vol. 181, pp. 291-328.

[102] Chen, S.; Yu, L.; Jiang, C.; Zhao, Y.; Sun, D.; Li, S.; Liao, G.; Chen, Y.; Fu, Q.; Tao, Q.; Ye, D.; Hu, P.; Khawli, L. A.; Taylor, C. R.; Epstein, A. L.; Ju, D. W. Pivotal study of iodine-131–labeled chimeric tumor necrosis treatment radioimmunotherapy in patients with advanced lung cancer. *J. Clin. Oncol.,* **2005**, *23* (7), 1538-1547.

[103] Epstein, A. L.; Chen, D.; Ansari, A.; Najafi, A.; Siegel, M.; Lee, K.; Hu, E.; Rosen, P.; Watkins, K.; Stain, S.; Weaver, F.; Taylor, C. R. Radioimmunodetection of necrotic lesions in human tumors using I-131 labeled TNT-1 F(ab′)2 monoclonal antibody. *Antibody. Immunoconj. Radiopharm.,* **1991**, *4*, 151-161.

[104] Miller, G. K.; Naeve, G. S.; Gaffar, S. A.; Epstein, A. L. Immunologic and biochemical analysis of TNT-1 and TNT-2 monoclonal antibody binding to histones. *Hybridoma,* **1993**, *12* (6), 689-698.

[105] Hornick, J. L.; Sharifi, J.; Khawli, L. A.; Hu, P.; Biela, B. H.; Mizokami, M. M.; Yun, A.; Taylor, C. R.; Epstein, A. L. A new chemically modified chimeric TNT-3 monoclonal antibody directed against DNA for the radioimmunotherapy of solid tumors. *Cancer Biother. Radiopharm.,* **1998**, *13* (4), 255-268.

[106] Street, H. H.; Goris, M. L.; Fisher, G. A.; Wessels, B. W.; Cho, C.; Hernandez, C.; Zhu, H. J.; Zhang, Y.; Nangiana, J. S.; Shan, J. S.; Roberts, K.; Knox, S. J. Phase I study of ^{131}I-chimeric(ch) TNT-1/B monoclonal antibody for the treatment of advanced colon cancer. *Cancer Biother. Radiopharm.,* **2006**, *21.* (3), 243-556.

[107] Hdeib, A.; Sloan, A. E. Convection-enhanced delivery of ^{131}I-chTNT-1/B mAB for treatment of high-grade adult gliomas. *Expert. Opin. Biol. Ther.,* **2011**, *11* (6), 799-806.

[108] Khawli, L. A.; Alauddin, M. M.; Hu, P.; Epstein, A. L. Tumor targeting properties of indium-111 labeled genetically engineered Fab′ and F(ab′)2 constructs of chimeric tumor necrosis treatment (chTNT)-3 antibody. *Cancer Biother. Radiopharm.,* **2003**, *18* (6), 931-940.

[109] Anderson, P. M.; Wiseman, G. A.; Lewis, B. D.; Charboneau, J. W.; Dunn, W. L.; Carpenter, S. P.; Chew, T. A phase I safety and imaging study using radiofrequency ablation (RFA) followed by ^{131}I-chTNT-1/B radioimmunotherapy adjuvant treatment of hepatic metastases. *Cancer Ther.,* **2003**, *1* (6), 297-306.

[110] Khawli, L. A.; Mizokami, M. M.; Sharifi, J.; Hu, P.; Epstein., A. L. Pharmacokinetic characteristics and biodistribution of radioiodinated chimeric TNT-1, -2, and -3 monoclonal antibodies after chemical modification with biotin. *Cancer Biother. Radiopharm.,* **2002**, *17* (4), 359-370.

[111] Zhang, N.; Sadun, R. E.; Arias, R. S.; Flanagan, M. L.; Sachsman, S. M.; Nien, Y. C.; Khawli, L. A.; Hu, P.; Epstein, A. L. Targeted and untargeted CD137L fusion proteins for the immunotherapy of experimental solid tumors. *Clin. Cancer Res.,* **2007**, *13* (9), 2758-2767.

[112] Sharkey, R. M. Radioimmunotherapy against the tumor vasculature: A new target?. *J. Nucl. Med.,* **2006**, *47* (7), 1070-1074.

[113] Chaplin, D. J.; Dougherty, G. J., Tumor vasculature as a target for cancer therapy. *Br. J. Cancer,* **1999**, *80*. (Suppl 1), 57-64.

[114] Siemann, D. W.; Bibby, M. C.; Dark, G. G.; Dicker, A. P.; Eskens, F. A.; Horsman, M. R.; Marmé, D.; LoRusso, P. M. Differentiation and definition of vascular-targeted therapies. *Clin. Cancer Res.,* **2005**, *11* (2 Pt 1), 416-420.

[115] Vincent, L.; Kermani, P.; Young, L. M.; Cheng, J.; Zhang, F.; Shido, K.; Lam, G.; Bompais-Vincent, H.; Zhu, Z.; Hicklin, D. J.; Bohlen, P.; Chaplin, D. J.; May, C.; Rafii, S. Combretastatin A4 phosphate induces rapid regression of tumor neovessels and growth through interference with vascular endothelial-cadherin signaling. *J. Clin. Invest.,* **2005**, *115* (11), 2992-3006.

[116] Hinnen, P.; Eskens, F. A. L. M. Vascular disrupting agents in clinical development. *Br. J. Cancer,* **2007**, *96* (8), 1159-1165.

[117] Shenoi, M. M.; Iltis, I.; Choi, J.; Koonce, N. A.; Metzger, G. J.; Griffin, R. J.; Bischof, J. C. Nanoparticle delivered vascular disrupting agents (VDAs): use of TNF-alpha conjugated gold nanoparticles for multimodal cancer therapy. *Mol. Pharm.,* **2013**, *10* (5), 1683-1694.

[118] Siemann, D. W. The unique characteristics of tumor vasculature and preclinical evidence for its selective disruption by tumor-vascular disrupting agents. *Cancer Treat. Rev.,* **2011**, *37,* 63-74.

[119] Horsman, M. R.; Siemann, D. W. Pathophysiologic effects of vascular-targeting agents and the implications for combination with conventional therapies. *Cancer Res.,* **2006**, *66* (24), 11520-11539.

[120] Chen, F.; Feng, Y.; Zheng, K.; de Keyzer, F.; Li, J.; Feng, Y.; Cona, M. M.; Wang, H.; Jiang, Y.; Yu, J.; Marchal, G.; Verfaillie, C.; de Geest, B.; Oyen, R.; Ni, Y. Enhanced antitumor efficacy of a vascular disrupting agent combined with an antiangiogenic in a rat liver tumor model evaluated by multiparametric MRI. *PLoS ONE,* **2012**, *7* (7), e41140.

[121] Hanahan, D.; Folkman, J. Patterns and emerging mechanisms of the angiogenic switch during tumorigenesis. *Cell,* **1996**, *86* (3), 353-364.

[122] Organ, L. W. Electrophysiologic principles of radiofrequency lesion making. *Appl. Neurophysiol.,* **1976-1977**, *39* (2), 69-76.

[123] Tabuse, Y.; Tabuse, K.; Mori, K.; Nagai, Y.; Kobayashi, Y.; Egawa, H.; Noguchi, H.; Yamaue, H.; Katsumi, M.; Nagasaki, Y. Percutaneous microwave tissue coagulation in liver biopsy: experimental and clinical studies. *Nihon. Geka. Hokan.,* **1986**, *55* (3), 381-392.

[124] Dodd, G. D. 3rd.; Soulen, M. C.; Kane, R. A.; Livraghi, T.; Lees, W. R.; Yamashita, Y.; Gillams, A. R.; Karahan, O. I.; Rhim, H. Minimally invasive treatment of malignant hepatic tumors: at the threshold of a major breakthrough. *RadioGraphics,* **2000**, *20* (1), 9-27.

[125] Giorgio, A.; Tarantino, L.; Francica, G.; Mariniello, N.; Nuzzo, A.; del Viscovo, L.; Rotondo, A. One-shot percutaneous ethanol injection of liver tumors under general anesthesia: preliminary data on efficacy and complications. *Cardiovasc. Intervent. Radiol.,* **1996**, *19* (1), 27-31.

[126] Sun, Z.; Ni, Y. Iodogen method for preparation of radioiodinated Hypericin. CN 200910013998, 2009.

[127] Cona, M. M.; de Witte, P.; Verbruggen, A.; Ni, Y. An overview of translational (radio)pharmaceutical research related to certain oncological and non-oncological applications. *World. J. Methodol.,* **2013**, *3* (4), 45-64.

[128] Loke, K. S.; Padhy, A. K.; Ng, D. C.; Goh, A. S. W.; Divgi, C. Dosimetric considerations in radioimmunotherapy and systemic radionuclide therapies: a review. *World. J. Nucl. Med.,* **2011**, *10* (2), 122-138.

[129] Cona, M. M.; Alpizar, Y. A.; Li, J.; Bauwens, M.; Feng, Y.; Sun, Z.; Zhang, J.; Chen, F.; Talavera, K.; de Witte, P.; Verbruggen, A.; Oyen, R.; Ni, Y. Radioiodinated hypericin: its biodistribution, necrosis avidity and therapeutic efficacy are influenced by formulation. *Pharm. Res.,* **2014**, *31* (2), 278-290.

[130] Cona, M. M.; Li, J.; Feng, Y.; Chen, F.; Verbruggen, A.; de Witte, P.; Oyen, R.; Ni, Y. Targetability and biodistribution of radioiodinated hypericin: comparison between microdosing and carrier-added preparations. *AntiCancer Agents. Med. Chem.,* **2014**, *14* (6), 852-861.

[131] Cona, M. M.; Koole, M.; Feng, Y.; Liu, Y.; Verbruggen, A.; Oyen, R.; Ni, Y. Biodistribution and radiation dosimetry of radioiodinated hypericin as a cancer therapeutic. *Int. J. Oncol.,* **2014**, *44* (3), 819-829.

[132] Seo, Y.; Gustafson, W. C.; Dannoon, S. F.; Nekritz, E. A.; Lee, C.L.; Murphy, S. T.; VanBrocklin, H. F.; Hernandez-Pampaloni, M.; Haas-Kogan, D. A.; Weiss, W. A.; Matthay, K. K. Tumor dosimetry using [^{124}I]m-iodobenzylguanidine microPET/CT for [^{131}I]m-iodobenzylguanidine treatment of neuroblastoma in a murine xenograft model. *Mol. Imaging. Biol.,* **2012**, *14* (6), 735-742.

[133] Cremonesi, M.; Bodei, M.; Rocca, P.; Stabin, M.; Maecke, M.; Paganelli, G. Kidney protection during receptor-mediated radiotherapy with ^{90}Y-[DOTA0, Tyr3]octreotide. *Cancer Biother. Radiopharm.,* **2002**, *17*, 344.

[134] Li, J.; Cona, M. M.; Chen, F.; Feng, Y.; Zhou, L.; Zhang, G.; Nuyts, J.; de Witte, P.; Zhang, J.; Yu, J.; Oyen, R.; Verbruggen, A.; Ni, Y. Sequential systemic administrations of combretastatin A4 phosphate and radioiodinated hypericin exert synergistic targeted theranostic effects with prolonged survival on SCID mice carrying bifocal tumor Xenografts. *Theranostics,* **2013**, *3* (2), 127-137.

[135] Bano, G.; Stanicova, J.; Jancura, D.; Marek, J.; Bano, M.; Ulicny, J.; Strejckova, A.; Miskovsk, P. On the diffusion of hypericin in dimethylsulfoxide/water mixtures—the effect of aggregation. *J. Phys. Chem. B.,* **2011**, *115* (10), 2417-2423.

[136] Van de Putte, M.; Roskams, T.; Bormans, G.; Verbruggen, A.; de Witte, P. A. M. The impact of aggregation on the biodistribution of hypericin. *Int. J. Oncol.,* **2006**, *28* (3), 655-660.

[137] Ji, Y.; Jiang, C.; Zhang, X.; Liu, W.; Gao, M.; Li, Y.; Wang, J.; Wang, Q.; Sun, Z.; Jiang, X.; Yao, N.; Wang, X.; Fang, Z.; Yin, Z.; Ni, Y.; Zhang, J. Necrosis-targeted combinational Theranostic approach to treat cancer. *Oncotarget,* **2014**, *5*(10), 2934-2946.

[138] Stoll, A.; Becker, B. Sennosides A and B, the Active Principles of Senna. In *Fortschritte der Chemie organischer Naturstoffe / Progress in the Chemistry of Organic Natural Products / Progrès dans la Chimie des Substances Organiques Naturelles.* Zechmeister, L., Ed. Springer Vienna: USA, **1950**, Vol. 7, pp. 248-269.

[139] Brans, B.; Bodei, L.; Giammarile, F.; Linden, O.; Luster, M.; Oyen, W. J.; Tennvall, J. Clinical radionuclide therapy dosimetry: the quest for the "Holy Gray". *Eur. J. Nucl. Med. Mol. Imaging,* **2007**, *34* (5), 772-786.

Received: August 17, 2014 **Revised: January 20, 2015** **Accepted: February 20, 2015**